

A DYNAMIC RESERVOIR SIMULATION MODEL - DYRESM: 5

Jörg Imberger and John C. Patterson

University of Western Australia
Nedlands, Western Australia

1. INTRODUCTION

The dynamic reservoir simulation model, DYRESM, is a one-dimensional numerical model for the prediction of temperature and salinity in small to medium sized reservoirs and lakes. The model was constructed to form a suitable basis for a more general water quality model. The requirements imposed by this aim are made by Imberger (1978), who shows that for both substances with a fast turnover time such as phytoplankton and for conservative substances such as salt, the mixing mechanisms within the reservoir must be modeled accurately. Not only must a model be capable of predicting the net cumulative vertical transfer of mass induced by the mixing and the subsequent flow processes, but it must also be capable of resolving individual mixing regions.

This is a great departure from what has been assumed to date. Previously it has been generally accepted that once a particular reservoir model was capable of being tuned to correctly predict the vertical temperature profiles over a particular study period, that this then constituted a reliable model for the purposes of water quality modeling. However, as discussed in Fischer *et al.*, (1979) this is not the case since different parameters are dependent on different mixing processes for their distribution.

The problem confronting the modeler is thus difficult. On the one hand the model should be widely applicable and cheap to run, and on the other it must capture the mixing induced by the small-scales of motion. The marriage of these seemingly conflicting aims requires careful consideration of not only the concept but also the architecture of a proposed model. Although increasing availability of computing power has led to an increased potential for application of two or three-dimensional reservoir models, the required resolution, down to centimeters and minutes, is not currently possible within the context of long term simulations, and a one-dimensional model appears to be the only realistic option.

The strong stratification normally found in small to medium sized reservoirs may be used to advantage. A strong stratification of the water inhibits vertical motions and reduces the turbulence to intermittent bursts. For such lakes the

A DYNAMIC RESERVOIR SIMULATION MODEL - DYRESM: 5

Jörg Imberger and John C. Patterson

University of Western Australia
Nedlands, Western Australia

1. INTRODUCTION

The dynamic reservoir simulation model, DYRESM, is a one-dimensional numerical model for the prediction of temperature and salinity in small to medium sized reservoirs and lakes. The model was constructed to form a suitable basis for a more general water quality model. The requirements imposed by this aim are made by Imberger (1978), who shows that for both substances with a fast turnover time such as phytoplankton and for conservative substances such as salt, the mixing mechanisms within the reservoir must be modeled accurately. Not only must a model be capable of predicting the net cumulative vertical transfer of mass induced by the mixing and the subsequent flow processes, but it must also be capable of resolving individual mixing regions.

This is a great departure from what has been assumed to date. Previously it has been generally accepted that once a particular reservoir model was capable of being tuned to correctly predict the vertical temperature profiles over a particular study period, that this then constituted a reliable model for the purposes of water quality modeling. However, as discussed in Fischer *et al.*, (1979) this is not the case since different parameters are dependent on different mixing processes for their distribution.

The problem confronting the modeler is thus difficult. On the one hand the model should be widely applicable and cheap to run, and on the other it must capture the mixing induced by the small-scales of motion. The marriage of these seemingly conflicting aims requires careful consideration of not only the concept but also the architecture of a proposed model. Although increasing availability of computing power has led to an increased potential for application of two or three-dimensional reservoir models, the required resolution, down to centimeters and minutes, is not currently possible within the context of long term simulations, and a one-dimensional model appears to be the only realistic option.

The strong stratification normally found in small to medium sized reservoirs may be used to advantage. A strong stratification of the water inhibits vertical motions and reduces the turbulence to intermittent bursts. For such lakes the

transverse and longitudinal direction play a secondary role and only the variations in the vertical enter the first order balances of mass, momentum and energy.

Departures from this state of horizontal isopycnals are possible, but these enter only as isolated events or as weak perturbations. In both cases the net effect is captured with a parameterization of their input to the vertical structure and a comparison of the model prediction and field data must thus be confined to periods of calm when the structure is truly one-dimensional.

The constraints imposed by such a one-dimensional model may best be quantified by defining a series of non-dimensional numbers. The value of the Wedderburn number

$$W = \frac{g'h}{u^{*2}} \cdot \frac{h}{L} \quad (1)$$

where g' is an effective reduced gravity across the thermocline, h the depth of the mixed layer, L the basin scale, and u^* the surface shear velocity, is a measure of the activity within the mixed layer. Spigel and Imberger (1980) have shown that for $W > 0(1)$ the departure from one-dimensionality is minimal and for $0(h/L) < W < 0(1)$ the departure is severe but may be successfully parameterized. For $W < 0(h/L)$ the lake overturns.

Inflows do not lead to severe vertical motions in the bulk of the reservoir provided the internal Froude number

$$F_i = \frac{U}{\sqrt{g'H}} < 1 \quad (2)$$

where U is the inflow velocity, g' the reduced gravity between the surface reservoir water and the inflow and H the reservoir depth.

The outflow dynamics is governed by a similar Froude number criterion

$$F_o = \frac{Q}{g'^{1/2}H^{5/2}} < 1 \quad (3)$$

where Q is the outflow discharge and g' the reduced gravity between the surface and bottom water.

Lastly, the earth's rotation will not lead to vertical motions if

$$\frac{g'\delta}{f^2B^2} < 1 \quad (4)$$

where g' is the effective reduced gravity over the depth δ , the scale of the velocity concentrations, f is the Coriolis parameter and B is the maximum width of the lake.

Within these constraints DYRESM yields an accurate description of the dynamics governing the vertical structure in a lake. It must, however, always be emphasized that superimposed on the structure predicted by DYRESM there are mixing processes which have only a second order influence on the vertical structures, but which are the first order mechanisms for transporting substances horizontally. These find their origins in enhanced heating and cooling at the edge of the lake, direct surface runoff, wind sheltering and shading by mountain ridges, and boundary mixing in the hypolimnion. Only the influence of these processes on the one-dimensional structure is modeled by DYRESM. A separate perturbation scheme is required to reveal their influence on horizontal variations in a reservoir. The first order vertical structure computed with DYRESM may in future investigations be used to compute such horizontal transport processes. These may be modeled with a simplified three-dimensional model using the one-dimensional vertical structure as the mean density field.

Even the one-dimensional problem is not simple. A uniform grid model which resolves these fine scales over the whole depth would require a large number of mesh points and computation would be slow, to say nothing about problems of stability and numerical diffusion. Even if local compaction of a wider grid were employed, which introduces its own problems, the model at any instant would have only an estimate of where the compaction was required for each process, and since several processes may occur at different positions simultaneously, little advantage would be gained.

With these considerations in mind, the model DYRESM was developed by Imberger *et al.* (1978) with a different approach to the task. Concentrating on parameterization of the physical processes rather than numerical solution of the appropriate differential equations, DYRESM makes use of a layer concept, in which the reservoir is modeled as a system of horizontal layers of uniform property. These layers move up and down, adjusting their thickness in accordance with the volume-depth relationship, as inflow and withdrawal increase and decrease the reservoir volume. In this way the problems of numerical diffusion associated with computation of vertical advection above the levels of inflow and withdrawal vanish.

There is, however, a far stronger reason for making use of adjustable layers as the model medium. Rather than being just a computational scheme, the layers may be given a functional character, and their dimension adjusted to suit the function expected of them. Thus the mixed layer, for example, may be modeled by a reasonably coarse layer structure in the epilimnion, fining down to very narrow layers in the transition zone. This adjustment of scale is performed by the algorithm itself, and thus only creates high resolutions when required. Further, by treating each of the dominant physical processes separately, only those layers affected by the process are operated on. In each of these process models, the proper range of scales may be accounted for and included explicitly.

The result of this concept is a model which is computationally very simple and yet conceptually more realistic than a fixed grid approach. Because of the computational simplicity, the algorithm is economical, and long term simulations which incorporate the finest scales become a realistic proposition.

2. DYRESM MAIN PROGRAM

The model DYRESM is constructed as a main program with subroutines which separately model each of the physical processes of inflow, withdrawal, mixed layer dynamics, and vertical transport in the hypolimnion. In addition, there are a number of service subroutines which provide maintenance of the layer system (volumes, positions, etc.) and provide calculations of physical properties which are frequently required such as density. The functions of the main program are therefore those of input/output, the calculation of fixed parameters, and control over timing of the calls to the various process subroutines.

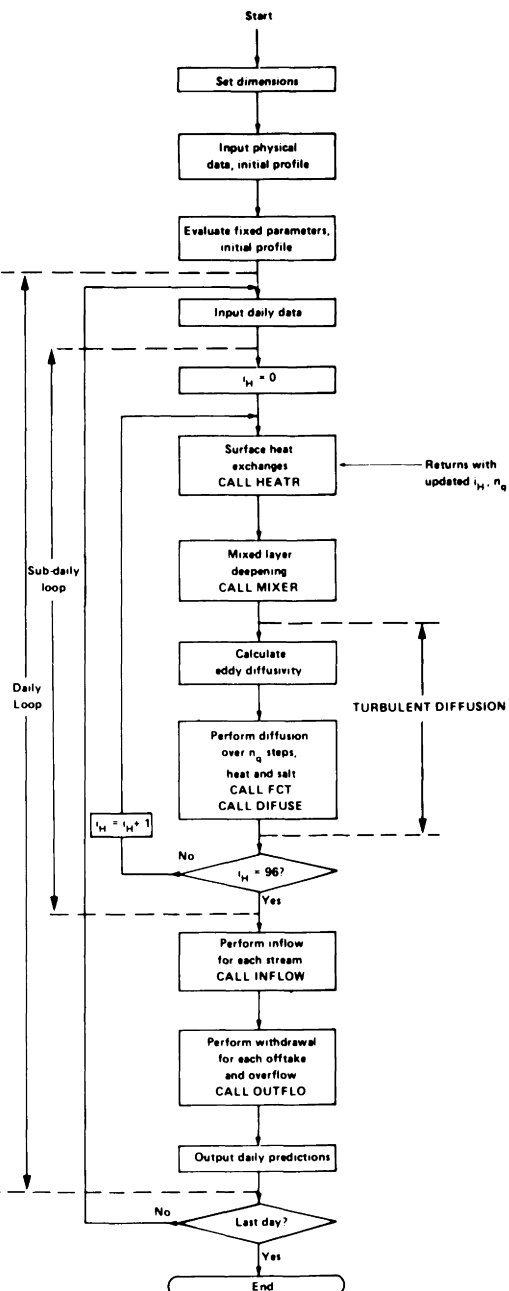
The question of how frequently the process subroutines should be called naturally arises. For most purposes, a daily prediction of the thermal structure is sufficient, and the basic time step of the model is set to this value. Since the inflow and outflow volumes change only slowly, generally over a few days at least, this basic time step is also suitable for these processes, and the appropriate subroutines are called once daily. On the other hand, the mixed layer dynamics covers scales very much shorter than one day, and even though daily averaged meteorological inputs are mostly used, the mixed layer model subroutines need to be called more frequently to match the response of the diurnal deepening.

Thus the model incorporates two time steps; a fixed basic step of one day and a variable sub-daily time step for the mixing algorithm. The length of this sub-daily step is determined by the dynamics and ranges between one quarter hour and twelve hours if averaged data is used. This procedure allows small time steps when the dynamics so require; in less critical periods, the time step expands without loss in accuracy.

DYRESM is then organized in the following way (see Flowchart 2.1). The main program inputs the fixed data; physical dimensions, volume and area as a function of depth, physical properties of the inflowing streams, locations of the offtakes, an initial temperature an salinity profile, and output control parameters.

The initial profile, yielded from field data, may not be of sufficient resolution. This is expanded by interpolation, a density profile computed, and the initial layer structure formed. Each point in the expanded profile becomes the top of an individual layer of uniform property. The layer volumes and areas are computed, and their size checked against preset criteria.

The daily loop begins with the input of the current inflow, withdrawal, and meteorological data. After some output, the sub-daily loop commences. An index i_H is set to zero, representing the start of the first quarter hour of the daily loop. Subroutine HEATR is called to model the surface heat exchanges and to determine the length of the sub-daily time step. This routine is described in Section 3.1; briefly, the time step length is determined by considering the heat input and the mixed layer velocity increase in one quarter hour period. The time step length is set by limiting these parameters to preset maximum values. The routine returns



Flowchart 2.1. DYRESM Mainline.

with i_H increased by the number of quarter hours in this time, and the algorithm proceeds.

The mixed layer dynamics is modeled by a call to MIXER, which internally calls the Kelvin-Helmholtz billowing routine KH. These subroutines are described in Section 3.2. The eddy diffusivity described in Section 3.3 is then computed in the main program and the diffusion routines FCT and DIFUSE (Section 3.4) called in one quarter hour time steps for the sub-daily period for both heat and salt. The counter i_H , incremented in HEATR, is checked against one day; if a day has not elapsed, control is looped back and the process repeated.

After completion of the sub-daily loop, subroutine INFLOW is called for each inflowing river. This subroutine is described in Section 3.5. Subroutine OUTFLO (Section 3.6) models withdrawal from each submerged offtake, and if necessary, flow over the crest. The model permits overflow only if the predicted surface level is above both the measured level and the crest level; the quantity of overflow permitted is that which restores the predicted level without overflow to the measured level. This action is taken because of the unreliable nature of most overflow volume data.

At this stage the predicted temperature and salinity structure is output, along with other information, and the daily loop is complete. If the simulation has reached the required day, the computation ceases. Otherwise the entire procedure is repeated.

The service subroutines THICK, RESINT, DENSTY and SATVAP are described in Section 3.7. Execution of the program requires 55K (octal) words of memory, and for the 964 day simulation of Wellington Reservoir, required 2300 seconds of CP time on a Cyber 73 at the West Australian Regional Computer Centre.

3. DYRESM SUBROUTINES

3.1 Surface Heat and Mass Exchange

3.1.1 Theoretical background. Profile data of the air temperature, humidity and wind speed above the lake surface are rarely available and the modeler must rely on single elevation data at a single station on or near the lake.

This fact necessitates the use of the following bulk aerodynamic formulae for the assessment of the fluxes of momentum, τ/ρ , heat, \tilde{H} , and moisture E

$$\frac{\tau}{\rho} = u^* u^* = C_D U^2 \quad (5)$$

$$\frac{\tilde{H}}{\rho c_p} = -u^* \theta^* = -C_H U (\theta - \theta_s) \quad (6)$$

$$\frac{E}{\rho} = -u^*q^* = -C_W U(q - q_s) \quad (7)$$

where C_D , C_H and C_W are the respective bulk transfer coefficients. The wind speed U , air temperature θ , and the humidity q are measured at some reference height, and the subscript s refers to a surface measurement.

Equilibrium turbulence theory indicates that the bulk transfer coefficients are not constant, but are dependent on the stability of the air. Several authors (Dear-dorff, 1968; Carson and Richards, 1978) have investigated this dependency. Rayner (1980) has summarized their findings, and established a relationship between the actual coefficient and its value under neutral conditions in terms of a bulk Richardson number. When applying this correction care must, however, be taken to ensure that the single point sensors, from which the data are obtained, are all well within the developing equilibrium boundary layer of the lake.

Two versions of DYRESM are currently available. A standard version which assumes neutral values of the coefficients C_D , C_H and C_W dependent only on the wind speed and an experimental version, developed by Rayner (1980), which uses Hick's (1975) iterative procedure to correct the fluxes for the air column stability. The latter algorithm first estimates the fluxes using neutral values of the coefficient. The fluxes so computed are used to calculate a first estimate of the Monin-Obukhov length. The self similar profiles of the meteorological boundary layer theory are then used to correct the initial estimates of the fluxes. This leads to an iterative process which normally converges very rapidly.

Several authors provide estimates of the 10 m neutral transfer coefficients C_D , C_H and C_W arising from extensive field measurements. In DYRESM it is assumed that the value of $C_D = 10^{-3}$ for $u < 5 \text{ ms}^{-1}$ but rising linearly to 1.5×10^{-3} for wind speed of 15 ms^{-1} (Hicks, 1972). The documented values of C_H and C_W range from 1.3×10^{-3} to 1.5×10^{-3} (Hicks, 1975; Pond *et al.*, 1974); a value of 1.4×10^{-3} is assumed.

In addition to the turbulent fluxes across the surface, heat transfers due to radiation must be considered. Long-wave radiation emitted from the water surface is given by (TVA 1972)

$$Q_{LR} = \epsilon \sigma T^4 \quad (8)$$

where ϵ is the emissivity ($=0.96$), σ the Stephan-Boltzman constant ($\sigma = 2.0411 \times 10^{-7} \text{ kJ/m}^2 \text{ hr} K^4$), and T the absolute temperature of the water surface. Some of this radiation is absorbed by atmospheric constituents and re-emitted back to earth. This atmospheric radiation is given by (Swinbank, 1963)

$$Q_{LA} = 0.937 \times 10^{-5} \sigma T_2^2 (1 - R_a) \quad (9)$$

where T_2 is the air temperature at 2 m height, and R the water surface reflectivity ($=0.3$). Field tests show this formula to be accurate to $\pm 12 \text{ W m}^{-2}$.

Clouds emit long-wave radiation and are accounted for by a factor in Eq. (9).

$$Q_{LAC} = (1 + 0.17C^2) Q_{LA} \quad (10)$$

where C is the part of the sky covered with clouds, measured in tenths of the total sky. It is assumed that Q_{LAC} is absorbed directly by the water in the upper surface slab.

On the other hand, short-wave solar radiation penetrates the surface and is absorbed within the water column, thereby heating it. Only the visible part of the solar spectrum (0.36 to 0.76 μ) penetrates below one meter and this serves as the definition of short-wave radiation. For depths greater than one meter the attenuation profile of this short-wave radiation is well described by Beer's Law

$$q(z) = Q_s e^{-\eta_1 z} \quad (11)$$

where Q_s is the solar radiation at the surface, z the depth, and η_1 the bulk extinction coefficient dependent on the turbidity of the water.

To describe attenuation over the full depth of water, account must be taken of the wavelength dependency of the extinction coefficient. The TVA (1972) report recommends use of three extinction coefficients, each associated with their own exponential decay. This option is included in DYRESM, but the actual attenuation profile and coefficient values used by DYRESM are dependent on the particular reservoir in question and must be specified by the user.

3.1.2 Surface heat and mass exchange algorithm. The heat exchanges through the surface are modeled by subroutine HEATR, which simulates radiation penetrative heating and the evaporative, conductive, and long-wave radiation exchanges at the surface.* These events are modeled by the bulk aerodynamic and radiation transfer formulae given by Eqs. (6) to (11).

The routine also sets the time step for itself and the following mixing and turbulent diffusion computations. As the short-wave radiation occurs only for half of the day, this time step is at most 12 hours. Further, to ensure that the turbulent velocity scale w^* and the mixed layer mean velocity U required by MIXER do not become excessively large, a further limit is imposed. This is set in the first case by limiting the change in surface temperature (before mixing) to a maximum of 3°C. This amounts to limiting the total \tilde{H}^* , and thus w^* , (defined in Section 3.2.1) for the total time step. In the second case, the mean velocity increase is limited to 1 cm/sec over the previous value, based on the previous mixed layer depth and the current value of u^* . The minimum time step set by these criteria is chosen down to a minimum of one quarter hour.

*Flow charts for all the subroutines mentioned in this section may be obtained by request to the authors.

Cooling at the surface or evaporation affect only the surface layer, and the density profile may be unstable following all the heat exchange occurring in a time step. HEATR makes no attempt to rectify this situation and merely passes the profile on to MIXER for stabilization.

The quarter hour time counter i_H is set to zero before the first call to HEATR. It is assumed that the short-wave radiation penetration occurs only for the second 12 hours of the day and thus is only applied if $i_H > 48$. The penetration law, Eq. (11), is applied, and the heat input to layer K evaluated as

$$\Delta Q_K = A_{K-1}\delta(Q_K) + (A_K - A_{K-1})Q_K \quad (12)$$

where A_K is the area of the layer, Q_K the radiation intensity arriving at the top of the layer determined by Eq. (11) and $\delta(Q_K) = Q_K - Q_{K-1}$

The evaporative, conductive and long-wave heat exchanges occur for all values of i_H and affect only the surface layer, layer NS . The heat input calculated from these effects is added to ΔQ_{NS} , and the temperature increment for each layer evaluated for a single quarter hour time step. Since the meteorological data responsible for these effects is averaged over a day, it is assumed that the temperature increment is a linear function of time and therefore that the 3°C change in surface temperature will occur in $n_q(T) = 3/|\Delta T|$ quarter hours, where ΔT is the surface change in one quarter hour, and n_q is rounded down, with a minimum value of one. Independently, the mean velocity criterion is given by $n_q(U) = 0.1h/u^{*2}$, where h is the mixed layer depth from the previous time step and u^* the current wind shear velocity; again n_q has a minimum value of one. The minimum of these two values is then taken as the number of quarter hours n_q for the current time step, i_H is incremented by n_q , cut off and n_q modified if the new i_H exceeds 48 or 96, and the total temperature increment for n_q quarter hours added into the temperature profile.

The salinity of the surface layer is adjusted for the effects of evaporation and rainfall, and finally a new density profile computed. Control is returned to the mainline ready for MIXER to be called.

3.2 Energetics of the Surface Layer

3.2.1 Theoretical background. Under the constraints given in the introduction the velocity and density distribution in the upper surface layer may be idealized as shown in Fig. 3.1. The velocity in the direction of the applied wind stress (ρu^{*2}) is characterized by a strong surface shear region near the water surface, with a thickness ranging from a few centimeters to one or two meters with increasing wind stress. Below this shear zone the velocity is relatively constant throughout the mixed layer. The mixed layer is defined as that surface water slab over which the water density is constant. Rayner (1980) has shown that this depth typically varies greatly within a day from zero to the depth of the seasonal thermocline. The momentum as well as the heat and mass introduced at the water surface are

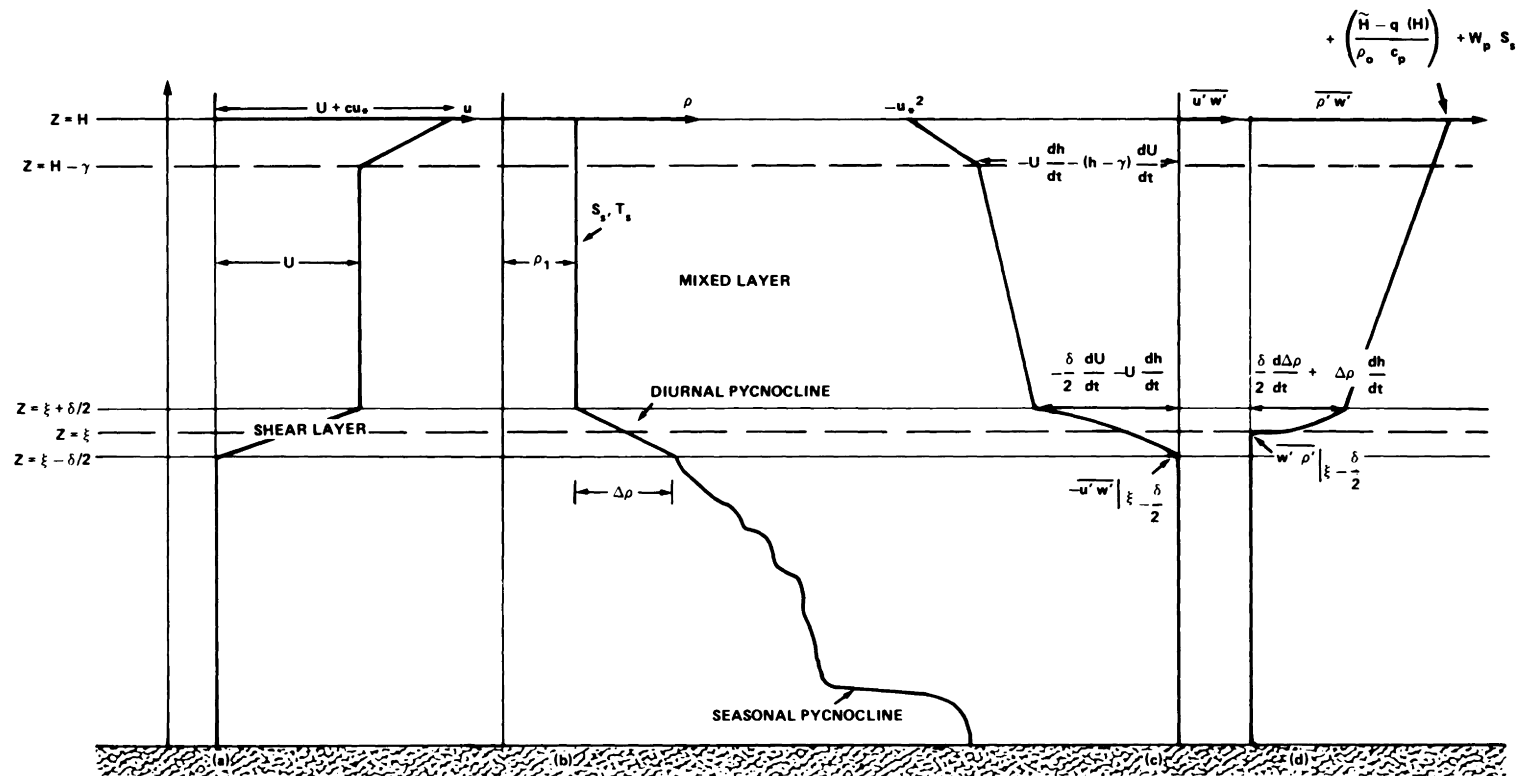


Figure 3.1. Model of the mixed layer and the assumed profiles of velocity, salinity, temperature, density, Reynolds stress and buoyancy flux.

continually being mixed or stirred into the surface mixed layer. The turbulent kinetic energy (T.K.E.) field will adjust to changes of the surface inputs in times of $O(h/u^*)$, where h is the mixed layer depth.

Consider first the behavior of this layer in the absence of horizontal pressure gradients which would normally be set up by the presence of the boundaries of the lake. With this simplification the momentum equation in any part of the profile reduces to (see Niiler and Kraus, 1977)

$$\frac{\partial u}{\partial t} = - \frac{\partial}{\partial z} (\bar{u}' w') \quad (13)$$

Integration of Eq. (13) from below the shear layer to any part of the profile, using the velocity distribution shown Fig. 3.1 yields the distribution of Reynolds stress sketched in Fig. 3.1.

The density profile shown in Fig. 3.1 allows a similar calculation of $\bar{w}' \rho'$ from the mass equation

$$\frac{\partial \rho}{\partial t} = - \frac{\partial}{\partial z} (\bar{\rho}' \bar{w}') - \frac{\alpha}{c_p} \frac{\partial q(z)}{\partial z} \quad (14)$$

where q is the radiation heat flux at a depth z .

To obtain the mechanical energetics of the mean flow Eq. (13) may be multiplied by the velocity u and integrated over the mixed layer. The balance so obtained shows that during deepening ($dh/dt > 0$) or billowing ($d\delta/dt > 0$) events, a certain amount of mean kinetic energy is lost both in the surface shear layer and in the base shear layer. As is shown in Lumley and Tennekes (1972) this energy change is not a loss, but merely a transfer to turbulent kinetic energy and therefore it must be accounted for in the TKE budget.

The total transfer of energy accomplished via this adjustment is given by

$$\int_{-\delta/2}^{\xi+\delta/2} \bar{u}' \bar{w}' \frac{du}{dz} dz + \int_{H-\gamma}^H \bar{u}' \bar{w}' \frac{du}{dz} dz = + \frac{\Delta U \delta}{6} \frac{d \Delta u}{dt} + \frac{1}{12} (\Delta U)^2 \frac{d \delta}{dt} \\ + \frac{(\Delta U)^2}{2} \frac{dh}{dt} + c u^{*3} + \gamma \frac{c u^*}{2} \frac{d \Delta U}{dt} \quad (15)$$

where ΔU is the velocity increment across the base of the mixed layer and c is a constant.

Similarly, the profile of $\bar{w}' \rho'$ shown in Fig. 3.1 leads to an adjustment of the mean potential energy of the mixed layer structure. During deepening and billowing the heavier fluid below the mixed layer is entrained into the base of mixed layer causing an adjustment of the profile shown in Fig. 3.1 with corresponding raising of the center of gravity of the water column and a rate of change of potential energy P.E. given by

$$\frac{d}{dt} \dot{P.E.} = -\frac{g}{2} \left\{ 2h \Delta \rho \frac{dh}{dt} + \frac{\delta \Delta \rho}{6} \frac{d\delta}{dt} + \left(h^2 + \frac{\delta^2}{12} \right) \frac{d}{dt} (\Delta \rho) \right\} \quad (16)$$

The above evaluations now allow an accounting of the turbulent kinetic energy budget expressed by the equation (see Denman, 1973)

$$\frac{1}{2} \frac{\partial \bar{E}}{\partial t} = - \overline{u'w'} \frac{\partial u}{\partial z} - \frac{\partial}{\partial z} \left| \overline{w' \left(\frac{p'}{\rho_0} + \frac{E}{2} \right)} \right| - \frac{g \overline{p'w'}}{\rho_0} - \epsilon \quad (17)$$

where $\bar{E}/2 = \overline{(u'^2 + v'^2 + w'^2)}/2$ is TKE per unit mass, $\overline{u'w'} \partial U / \partial z$ is the shear production of TKE by Reynolds stresses $\overline{u'w'}$ and velocity shear of the mean flow $\partial u / \partial z$, $\partial / \partial z [w'(p'/\rho_0 + E/2)]$ is transport of TKE by vertical velocity fluctuations w' , $g \overline{p'w'}/\rho_0 = g(-\alpha \theta' w' + \beta s' w')$ is the work done locally against buoyancy forces by TKE lifting heavier fluid (α, β are compressibilities for heat and salt; p', θ', s' are density, temperature and salinity fluctuations, respectively), and ϵ is the dissipation of TKE by viscosity. Equation (17) is valid at any point in the water column and may be integrated from the base of the thermocline $z = \xi - \delta/2$ to the water surface $z = H$ using the assumed profiles of Fig. 3.1, with a finite thermocline thickness δ .

Making use of the integrated equations for heat and mass as well, the integrated TKE budget may be written as

$$\begin{aligned} & \frac{1}{2} \frac{\partial}{\partial t} (E_S h) + \left\{ \frac{gh \Delta \rho}{2\rho_0} \frac{dh}{dt} + \frac{g\delta^2}{24\rho_0} \frac{d}{dt} \Delta \rho + \frac{g\delta \Delta \rho}{12\rho_0} \frac{d\delta}{dt} \right\} = \\ & \quad 1 \qquad \qquad \qquad 2 \\ & + \left\{ \frac{\Delta U \delta}{6} \frac{d\Delta U}{dt} + \frac{1}{12} \Delta U^2 \frac{d\delta}{dt} + \frac{\Delta U^2}{2} \frac{dh}{dt} \right\} + \frac{c}{2} u^{*3} \\ & \quad 3 \qquad \qquad \qquad 4 \\ & - \left. \overline{w' \left(\frac{p'}{\rho_0} + \frac{E}{2} \right)} \right|_H + \frac{\alpha g h \tilde{H}^*}{2\rho_0 C_p} + \frac{\beta g h \tilde{S}_S}{2} - \left. \frac{g(h+\delta) \overline{p'w'}}{2\rho_0} \right|_{\xi-\delta/2} \\ & \quad 5 \qquad \qquad \qquad 6 \qquad \qquad \qquad 7 \qquad \qquad \qquad 8 \\ & + \left. \overline{w' \left(\frac{p'}{\rho_0} + \frac{E}{2} \right)} \right|_{\xi-\delta/2} - \epsilon_s (h+\delta/2) - \left. \overline{u'w'} \right|_{\xi-\delta/2} \Delta U \\ & \quad 9 \qquad \qquad \qquad 10 \qquad \qquad \qquad 11 \end{aligned} \quad (18)$$

Each term and its related scales are as follows:

1. Rate of change of depth integrated TKE, as determined by the various sources and sinks of TKE on the right hand side of the equations. E_S is the depth integrated TKE in the mixed layer. Since turbulence is generated by both wind and convective overturn, we introduce the scale q^* incorporating both these effects (see also Zeman and Tennekes, 1977)

$$q^{*3} = w^{*3} + \eta^3 u^{*3} \quad (19)$$

where now

$$w^{*3} = \frac{\alpha g h \tilde{H}^*}{\rho_o c_p} + \beta g h \tilde{W} S_S \quad (20)$$

is modified to include the effects of evaporation at the surface, which leaves a residue of heavier, saltier water at the surface. \tilde{H}^* is net surface cooling corrected for the stabilizing effects of solar radiation absorption, as described below in connection with term 6. Hence, $E_S \sim q^{*2}$ and $\partial(E_S h)/\partial t \sim q^{*2} dh/dt$.

2. Rate of change of potential energy due to deepening and billowing. Billowing is due to shear instability at the base of the mixed layer.
3. Shear production within the lower shear layer.
4. Shear production within the surface shear layer.
5. Downward transport by vertical velocity fluctuations of TKE input at the free surface. Terms 4 and 5 both scale with u^{*3} and are the sources of TKE for the wind stirring mechanism.
6. TKE produced by convective overturn resulting from surface cooling, corrected for the effects of solar radiation. \tilde{H}^* is defined by

$$\frac{\tilde{H}^*}{\rho_o c_p} = \overline{\theta' w'}(H) + q(H) + q(\xi) - \frac{2}{h} \int_{\xi}^H q(z) dz \quad (21)$$

$\overline{\theta' w'}(H)$ is the net heat exchange that occurs just at the water surface, including all turbulent and long-wave radiative transfers. $q(z)$ is the solar radiation flux in the water. The three solar radiation terms in Eq. (21) account for the stabilizing effect on the water column of the exponential attenuation of solar radiation with depth. Whereas $\overline{\theta' w'}(H)$ is a source of TKE for net cooling, $q(H) + q(\xi) - 2/h \int_{\xi}^H q(z) dz$ will be a sink for TKE if the $q(z)$ profile is concave downward, as is usually the case. This may be better understood by considering the thermal energy equation

$$\frac{\partial T}{\partial t} = - \frac{\partial \overline{\theta' w'}}{\partial z} - \frac{1}{\rho_o C_p} \frac{\partial q}{\partial z} \quad (22)$$

If $q(z)$ is a linear function of z , then $\partial q/\partial z = \text{constant}$ so that heating of the water column $\partial T/\partial t$ by solar radiation will be uniform with depth, with no net stabilizing or destabilizing effects produced. (Note that for $q(z)$ linear, the solar radiation terms in Eq. (21) sum to zero). As Rayner (1980) points out, the form of Eq. (21) emphasizes the importance of correct modeling of solar radiation absorption for mixed layer energetics. Finally, we note that term (6) can be a sink for TKE if \tilde{H}^* is negative (net heating).

7. TKE produced by convective overturn due to salinity increases caused by evaporation. Terms 2, 6 and 7 result from the integral

$$\int_{\xi-\delta/2}^H \overline{w' \rho'} dz$$

8. Leakage of turbulent fluxes of heat and salt from the mixed layer into the hypolimnion

$$\frac{\rho' w'}{\rho_0} \Big|_{\xi-\delta/2} = (-\alpha \overline{\theta' w'} + \beta \overline{s' w'}) \Big|_{\xi-\delta/2}$$

is a sink for mixed layer TKE.

9. Downward transport by vertical velocity fluctuations of TKE into the hypolimnion. As with

$$\overline{u' w'} \Big|_{\xi-\delta/2} \Delta U$$

term 9 may act as a source for internal waves in the hypolimnion and is a sink for mixed layer TKE.

10. Depth integrated dissipation in the mixed layer, $\epsilon_S \sim q^{*3}/h$.

11. Rate of working by the lower shear layer on the hypolimnion.

Using the scales given above we introduce the following parameterization

$$\frac{1}{2} \frac{d(E_S h)}{dt} = C_T q^{*2} \frac{dh}{dt} \quad (23)$$

$$\frac{cu^{*3}}{2} - \overline{w' \left(\frac{p'}{\rho_o} + \frac{E}{2} \right)} \Big|_H - \epsilon_S(h+\delta/2) = \frac{C_K}{2} \eta^3 u^{*3} \quad (24)$$

$$\frac{\alpha g h \tilde{H}^*}{2\rho_o c_p} + \frac{\beta g h W S_S}{2} = \frac{w^{*3}}{2} \quad (25)$$

$$\begin{aligned} & \frac{gh \overline{p' w'}}{2\rho_0} \Big|_{\xi-\delta/2} + \overline{u' w'} \Big|_{\xi-\delta/2} \Delta U + \overline{w' \left(\frac{p'}{\rho_o} + \frac{E}{2} \right)} \Big|_{\xi-\delta} - \epsilon_S(h+\delta/2) \\ &= \Lambda_L + (1-C_K) \frac{q^{*3}}{2} \end{aligned} \quad (26)$$

Substituting Eq. (19) to Eq. (26) into the TKE budget Eq. (18), rearranging terms, and writing the result in finite difference form gives

$$\begin{aligned} & \left[\frac{C_T}{2} q^{*2} + \frac{\alpha \rho g h}{2\rho_0} + \frac{g \delta^2}{24\rho_0} \frac{d \Delta \rho}{dh} + \frac{g \Delta \rho \delta}{12\rho_0} \frac{d \delta}{dh} \right] \Delta h \\ & \quad 1 \qquad \qquad \qquad 2 \\ &= \frac{C_K}{2} (w^{*3} + \eta^3 u^{*3}) \Delta t + \\ & \quad 3 \qquad \qquad \qquad 4 \\ & \frac{C_S}{2} \left[\Delta U^2 + \frac{\Delta U^2}{6} \frac{d \delta}{dh} + \frac{\Delta U \delta}{3} \frac{d \Delta \delta}{dh} \right] \Delta h - \Lambda_L \Delta t \\ & \quad 5 \qquad \qquad \qquad 6 \end{aligned} \quad (27)$$

$\Delta \rho$ is now the density difference between the mixed layer and the next layer of thickness Δh . The left hand side of Eq. (27) gives the energy required in time Δt to entrain the next layer, while the right hand side gives the energy available for mixing. C_T, C_K, η and C_S are 0(1) coefficients related to the efficiencies involved in the mixed layer energetics; their values as determined by experiment are discussed in Section 4. For the solution of the problem Eq. (27) must be solved simultaneously with an equation for the velocity shear ΔU and the billow thickness δ .

The characteristics of the billowing have recently been documented in the laboratory by numerous investigators. Corcos and Sherman (1976) discuss an inviscid model and Thorpe and Hall (1977) have given evidence of their effect in Loch Ness. However, the processes involved during the latter stages of the instability and the subsequent mixing has still yet to be resolved. Much of this work is

summarized in Corcos (1979) who suggests the time scale for billowing, collapse and re-establishment of a new mean density profile is given by

$$T_B = \frac{20\Delta U}{g'} \quad (28)$$

Even with severe billowing this time is quite short typically being of order 10 - 60 seconds. This means that an interface which has been sharpened by the erosion from surface stirring energy source will retain a billowed interface with an interface width δ characterized by

$$\delta = \frac{0.3(\Delta U)^2}{g'} \quad (29)$$

Since the shear ΔU changes on a much slower time scale than this, the interface thickness will be modulated by the time scale of the shear and

$$\frac{d\delta}{dt} = \frac{0.6\Delta U}{g'} \frac{d(\Delta U)}{dt} - \frac{0.3(\Delta U)^2}{g'^2} \frac{dg'}{dt} \quad (30)$$

where the variation of g' can often be neglected over a time scale relevant for the shear.

Lastly, an equation for ΔU must be derived from the momentum Eq. (13), but with the pressure gradient added. In principle, this would involve a rather lengthy computation of the velocity field at each time step. In the construction of DYRESM it was felt that while it was important to include the parameterization of the shear production as this is responsible for the majority of the deepening during severe storms, it would be computationally too time consuming to solve for the full velocity field in the reservoir even when Coriolis accelerations are neglected.

A very simple parameterization of the integral of momentum equation for the mixed layer only presents itself. It basically consists of assuming that the integral to Eq. (13) at the center of the lake is given by

$$\Delta U = \frac{u^{*2}t}{h} \quad (31)$$

for a time before the internal waves generated by the end boundaries have propagated to the center of the lake and set up the pycnocline. In Fischer, *et al.*, (1979) it is shown that this occurs in a time of one quarter of the internal wave period. Beyond this time the shear across the interface will oscillate and decay to zero as dissipation takes effect. Thus a simple linear increase with a full cut off of the shear is conceptually the simplest representation of the actual behavior of the momentum. This idea was incorporated in DYRESM by Spigel (1978) and includes provision for a variable wind and an effective dissipation time.

3.2.2 Mixed layer dynamics algorithm. The mixed layer dynamics are simulated by subroutines MIXER and KH, which determine the mixed layer deepening and the Kelvin-Helmholtz billowing at the interface respectively. The routines are based on Eqs. (27), (30) and (31). The algorithm acts on the density profile generated by heat transport subroutine HEATR. As this profile is the result of both surface heat exchanges and penetrative heating from radiation, there may be a density instability present at the surface. Stabilization of this profile is equivalent to the calculation of the buoyancy flux and the total distributed heat flux \tilde{H}^* . Since evaporative losses are also included, w^* may be directly calculated from Eq. (20), or alternatively, from an equivalent mean potential energy formulation. If no surface cooling has occurred, the profile will not require stabilization, the mixed layer depth becomes the top model layer thickness, and $w^* = 0$.

The simplest possible solution of Eq. (27) would be an explicit evaluation of all of the available energies in a time step concerned with the mixing of a particular layer, followed by a comparison with the required energy, with the process applied layer by layer until the available energy is exhausted. The difficulty here is that in cases of high wind stress and small mixed layer depth, an excessively high shear velocity is produced in the fixed time step Δt . In these cases, the time step needs to be reduced below that set by HEATR. In the context of DYRESM, this is undesirable.

To avoid this problem, the balance described by Eq. (27) is applied in sections. Firstly, the deepening by stirring alone is applied layer by layer until there is insufficient energy available for further deepening. To the residual is added energy made available from shear production and billowing during this initial deepening after an adjustment of the shear velocity via Eq. (31). Deepening by shear production and billowing is then applied to further layers by again comparing the available energy, including the residual, to that required. At each incremental deepening, all of the variables are updated to their current values.

The resulting interface is then opened an amount corresponding to the shear instability for the time step by subroutine KH, which evaluates the size of the Kelvin-Helmholtz billows. If these meet certain size and time criteria, the sharp interface is relaxed over the billow thickness.

Thus the mixed layer dynamics is modeled in four distinct sections; deepening by convective overturn, deepening by stirring, deepening by shear production which includes continual readjustment of the shear velocity, and mixing of the pycnocline by Kelvin-Helmholtz billows.

The routine MIXER is called with the density profile stored in model layers 1 to NS, where layer NS is the surface layer, with the residual energy available for mixing from the previous step, and with the various parameters from the previous step required by the shear production algorithm.

Convective overturn. The density of layer NS is checked against that of layer NS-1; if an instability exists, the layers are mixed, a new density computed and compared with layer NS-2. The process is repeated until a stable gradient is achieved. Each such mixing releases a quantity of potential energy, and the corresponding turbulent velocity scale w^* is calculated. This potential energy for-

mulation of w^* may be equated with the TKE form Eq. (20). If layers K , $K+1$, \dots , NS have mixed, w^* is then given by

$$w^{*3} = \frac{g}{\rho_f \Delta t} \left\{ \sum_{i=K}^{NS} \frac{\rho_i (d_i - d_{i-1}) (d_i + d_{i-1})}{2} - \frac{(d_{NS} + d_{K-1})}{2} \sum_{i=K}^{NS} \rho_i (d_i - d_{i-1}) \right\} \quad (32)$$

where ρ_i is the density and d_i the height of the top of the i^{th} layer, and ρ_f the density of the mixed layers. The mixed layer depth becomes $h = d_{NS} - d_{K-1}$. Should the mixed layer deepen to the bottom the time counter is incremented and control is returned to the main program with reinitialized velocity and residual energy.

Stirring. With the evaluation of w^* from the stabilization section complete, the total energy made available for mixing by stirring in a single time step Δt is calculated. To this is added any residual available energy from the previous time step. Thus the total available energy from stirring mechanisms becomes

$$E_a = \frac{C_K q^3 \Delta t}{2} + E_a \quad (33)$$

where q is given by Eq. (19)

The energy required to mix layer $K-1$ is given by

$$E_r = \left(\frac{\Delta \rho}{\rho} gh + C_T q^2 \right) \frac{\Delta h}{2} \quad (34)$$

where $\Delta h = d_{K-1} - d_{K-2}$ the thickness of layer $K-1$ and $\Delta \rho/\rho = 2(\rho_{K-1} - \rho_f)/(\rho_{K-1} + \rho_f)$. The layer is mixed if $E_a \geq E_r$, in which case a new ρ_f is calculated, K decremented, E_a reduced by an amount E_r , and new values of $\Delta \rho/\rho$ and Δh established. The process is repeated until $E_a < E_r$, at which stage the mixed layer has deepened by a further amount \tilde{h} . Thus the total mixed layer depth is now

$$h = h + \tilde{h} + d_{NS} - d_{K-1} \quad (35)$$

Again, if deepening is vigorous enough for the mixed layer to reach the bottom, the algorithm is complete and control is returned after incrementing the time counter and reinitializing the velocity and energy residual.

Shear production. The deepening resulting from shear at the interface requires the solution of Eq. (31) for the mean velocity shear ΔU . The precomputation of mixing by the stirring mechanism ensures that in times of high wind stress the mixed layer depth will also be relatively large, and the resultant shear

velocity remains at a sensible level. The procedure for determining the mean velocity is a complex one and is discussed fully by Spigel (1978). Briefly, the procedure is as follows.

Equation (31) yields a linear growth in ΔU with time for a fixed u^* , up to an effective cut off time t_{eff} at which time ΔU falls to zero. The cut off time assumes use only of the energy produced by shear at the interface during the first wave period T_i , and thus is defined by

$$\int_0^{t_{eff}} \left(\frac{u^{*2} t}{h} \right)^2 dt = \int_0^{T_i} u^2 dt = 4 \int_0^{T_i/4} \left(\frac{u^{*2} t}{h} \right)^2 dt \quad (36)$$

where T_i is calculated for an equivalent two layer profile and no damping is assumed. This yields

$$t_{eff} = 1.59 T_i / 4 \quad (37)$$

Spigel (1978) inserts a correction for damping to yield

$$t_{eff} = \frac{T_i}{4} \left[0.59 \left\{ 1 - \operatorname{sech} \left(\frac{T_d}{T_i} - 1 \right) \right\} + 1 \right] \quad (38)$$

where L_d is the damping time for the equivalent two layer system. Thus the shear velocity is effectively given by

$$\begin{aligned} \Delta U &= \frac{u^{*2} t}{h} + \Delta U_o & t \leq t_{eff} \\ \Delta U &= 0 & t > t_{eff} \end{aligned} \quad (39)$$

where ΔU_o is the last value of ΔU and, since t_{eff} may extend over more than one day, u^* may be a function of time. Once cut off has occurred, ΔU remains zero until a change in wind stress occurs.

Thus the algorithm requires the last value of ΔU from the previous time step and a time counter to determine the position of the current time relative to t_{eff} . The previous value of the slope of the velocity function u^{*2}/h is also required to determine a new start up time. The slope of the function may of course change within one period of t_{eff} as the wind stress changes from day to day.

With the procedure for establishing ΔU within a time step, the algorithm proceeds in the following manner. The shear velocity computed in the previous time step is adjusted for the new mixed layer depth from momentum considerations. This adjusted value is used as an initial value and the layer accelerated with acceleration u^{*2}/h over the time step Δt or, if cut off occurs before Δt , until t_{eff}

is reached. An average velocity for the time step is formed

$$U_{av} = \frac{1}{\Delta t} \int_0^t \Delta U \, dt \quad (40)$$

This velocity is used to evaluate the energy produced by shear and billowing during the stirring phase, given by

$$\begin{aligned} E_a = & \frac{C_S}{2} \left[U_{av}^2 \tilde{h} + \frac{U_{av}^2 \Delta(\delta)}{6} + \frac{U_{av} \delta \Delta(U_{av})}{3} \right] \\ & + \left[g \frac{\Delta\rho}{\rho} \frac{\delta^2 \tilde{h}}{24h} - g \frac{\Delta\rho}{\rho} \frac{\delta \Delta(\delta)}{12} \right] \end{aligned} \quad (41)$$

where $\Delta(U_{av})$ is the change in U_{av} from the previous time step, $\Delta(\delta)$ is the current billowing thickness change given by

$$\Delta(\delta) = \frac{0.6 U_{av} \Delta(U_{av})}{g \Delta\rho / \rho} \quad (42)$$

To this energy is added any residual energy from the previous phase.

The algorithm now considers the mixing of the next layer, layer $K-1$. From shear production, additional energy

$$\begin{aligned} E_a = & \frac{C_S}{2} \left[U_{av}^2 \Delta h + \frac{U_{av} \Delta(\delta)}{6} + \frac{U_{av} \delta \Delta(U_{av})}{3} \right] \\ & + \left[g \frac{\Delta\rho}{\rho} \frac{\delta^2 \Delta h}{24h} - g \frac{\Delta\rho}{\rho} \delta \frac{\Delta(\delta)}{12} \right] \end{aligned} \quad (43)$$

is available, where $\Delta h = d_{K-1} - d_{K-2}$. The energy required is again given by

$$E_r = \left(g \frac{\Delta\rho}{\rho} + C_T q^2 \right) \frac{\Delta h}{2} \quad (44)$$

Layer $K-1$ is mixed if $E_a \geq E_r$, in which case K is decremented, a new density computed, E_a reduced by an amount E_r , U_{av} adjusted for the deeper mixed layer, and δ and $\Delta\rho/\rho$ recalculated. The process is then continued, with $\Delta(U_{av})$ and $\Delta(\delta)$ being the changes in U_{av} and δ from the previous comparison. The loop concludes when $E_a < E_r$ for some layer, or the deepening has reached the bottom, in which case control is passed back to the main program, after incrementing

the time counter and reinitializing the velocity and residual. Any residual E_a is stored for use in the following time step.

Billowing. The interface resulting from the mixing phases above is unstable to shear if its thickness has been reduced below that given by Eq. (29). In this case Kelvin-Helmholtz billows will be formed. This is accounted for by a call to subroutine KH, which evaluates a billow scale given by Eq. (29). If the billows are of sufficient thickness, at least six layers are formed over the shear zone, incorporating or splitting existing layers as required. These layers are then successively mixed from the interface out, yielding an approximately linear density gradient across the billow thickness. If the billows are of insufficient size, the interface is unaffected.

The final act of KH is to coalesce all the layers above the shear zone into a single large layer to facilitate computation in the following stages of the main program. Control then returns to MIXER, which runs a final check on the density profile stability before returning control to the main program.

3.3 Vertical Diffusion in the Hypolimnion

3.3.1 Theoretical background. The vigorous mixing in the epilimnion has been parameterized in Section 3.2, and this allows the calculation of the depth of the thermocline. The waters of the hypolimnion are protected by the thermocline from disturbances above. In addition, the density gradient in the hypolimnion, although weak, has a stabilizing effect, and it may be expected that vertical mixing in the hypolimnion is small, perhaps only on a molecular level.

There have been many studies in which the evolution within the hypolimnion of concentration distributions of natural or artificially introduced tracers have been measured. Fischer, *et al.*, (1979) summarize the results of these studies and conclude that there is evidence of relatively vigorous, but isolated, mixing in the hypolimnion. The only explanation for such patchy mixing is that although there is not sufficient kinetic energy to cause overall mixing, there are areas in the lake at any particular time where the energy density has been increased by some type of concentrating mechanism allowing a local breakdown and mixing of the structure.

The mixing mechanisms are most likely varied from one lake to the next, but it appears (see Garrett, 1979) that they fall into three major classes. First, internal wave interaction leads, under the right conditions, to a growth of one wavelength at the expense of the others until breaking occurs. These interactions may involve triads of internal waves, parametric instabilities or wave-wave shear interaction. Second, the local shear may be raised, by the combining of long and short internal waves, to such a level that Kelvin-Helmholtz billowing can take place. Thirdly, gravitational overturning can be induced by absorption of wave energy at critical layers.

Regardless of the mechanism responsible, mixing in a stratified fluid is characterized by an overturning motion with a scale of at most a few meters (see Fig. 3.2a). The energetics of the mixing has so far not been explained in any

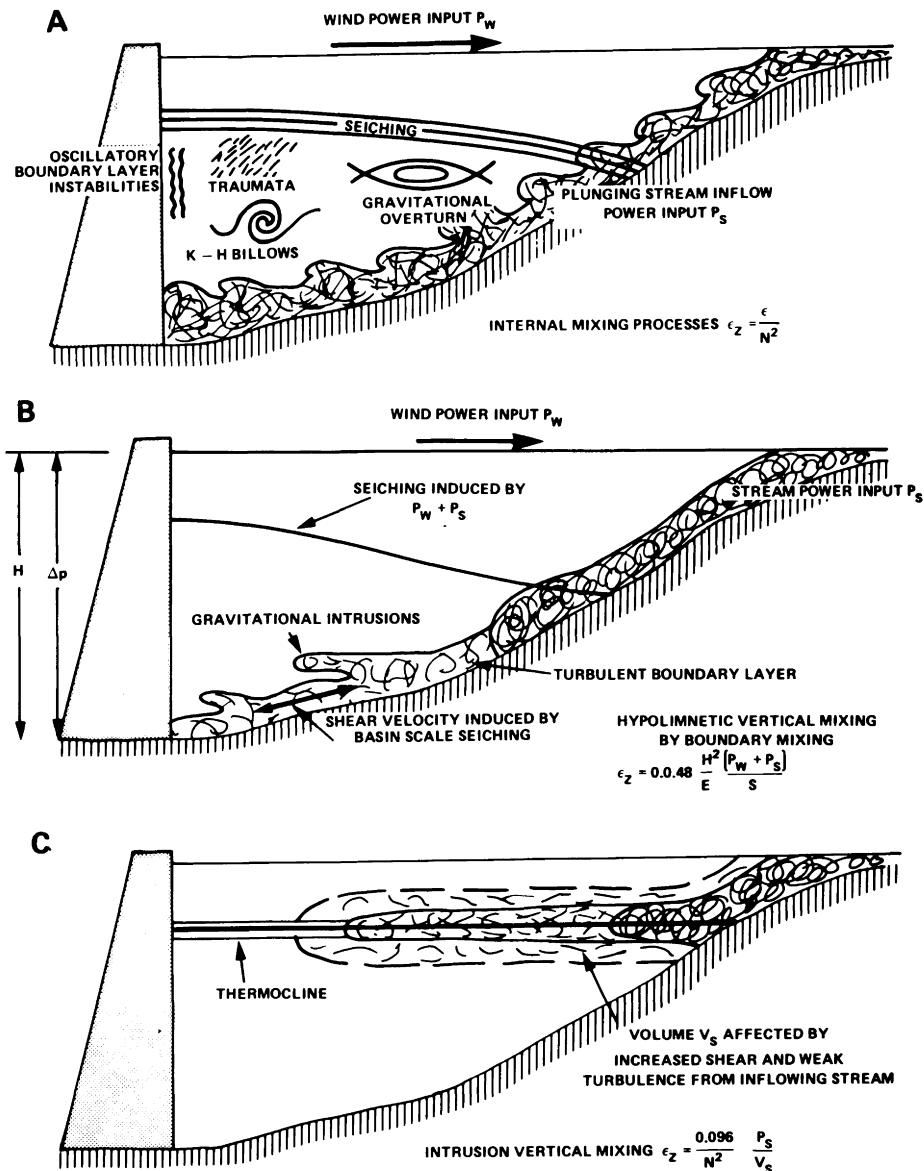


Figure 3.2. (a) Model of basin scale mixing in the hyplimnion of a lake. Wind and river inflow induce basin scale motions which in turn induce internal as well as boundary mixing. (b) Boundary mixing model. The vertical structure is actually adjusted via laminar horizontal intrusions which are driven by boundary mixing. (c) Local river induced mixing. A river intrusion often takes place near the seasonal thermocline, with little associated basin scale oscillation. Such intrusions do, however, induce mixing immediately below and above the intrusion.

detail, but in general the energy introduced by the wind at the lake surface or by the inflow in tumbling to a depth within the lake, induces mean motions and internal waves with scales ranging from the basin size to a few centimeters. These non-mixing motions interact in the hypolimnion until locally one of the above mechanisms leads to a local overturning event with subsequent mixing. The turbulent motions within the mixing patch lead to a readjustment of the potential energy. The remainder of the mean kinetic energy is either dissipated or radiated away by internal waves generated by the collapsing mixed patch. The local increase in potential energy caused by the mixing is in turn utilized to drive horizontal intrusions which are ultimately responsible for the adjustment of the mean density profile in the hypolimnion.

Garrett and Munk (1975) postulate a spectrum of internal waves truncated to allow the right amount of mixing for the particular external energy inputs. The presence of the external lake boundaries prohibits the direct application of the Garrett and Munk (1975) spectrum since, in lakes, one of the dominant mixing mechanisms appears to be the dissipation of basin scale seiching by turbulent boundary layers at the boundary of the lake (Fig. 3.2b). Here, the concept of equilibrium mixing related to the local gradients via the Cox number has only local significance. A simple dimensional argument may be used to derive an effective diffusion coefficient resulting from the general interaction between localized mixing and subsequent gravitational adjustment of the mixed patches.

Let P_W be the power introduced by the wind at the surface of the lake, P_S the power introduced by the inflowing streams and E the potential energy of the stratification in the whole lake. Then the global vertical diffusion coefficient ϵ_z may be written as

$$\epsilon_z = \alpha_1 \frac{H^2(P_W + P_S)}{ES} \quad (45)$$

where α_1 is a function depending on the basin shape, the stratification and the forcing history and S is a stability parameter $H/\Delta\rho dp/dz$ providing a local variation of ϵ_z with N^{-2} as indicated by experimental evidence. H is the depth of the lake and $\Delta\rho$ is the total density difference between the epilimnion and the hypolimnion. The formulation expressed by Eq. (45) has the advantage that it is simple, yet accounts for the energy input in a fashion similar to the more complicated spectral models and in addition the potential energy parameter E introduces a first order dependence on the basin shape.

Experience with DYRESM has indicated that α_1 may be taken as a constant ($= 0.048$) provided the lake hydrography is not too contorted. However, while Eq. (45) appears to describe the variation of the vertical transport coefficient of heat and mass due to mixing induced by basin scale motions, the simulation of Lake Argyle has indicated that the assumption that the power P_S is spread uniformly over the volume of the lake is not always valid. River inflows which do not plunge to great depth, but which intrude horizontally just above or below the thermocline, do not induce seiching, but rather merely cause local turbulence and shear within the intrusion itself (Fig. 3.2c).

Such a process suggests a diffusion coefficient formulation as proposed by Ozmido (1965) and we may postulate a local diffusion coefficient

$$\epsilon_z = \frac{\bar{\epsilon}}{N^2} \quad (46)$$

where $\bar{\epsilon}$ is the local dissipation. Once again if equilibrium flow is assumed an estimate for $\bar{\epsilon} = \alpha_2 P_S / V_S$, where V_S is the volume of the reservoir effected by the stream intrusion.

At present DYRESM uses the diffusion coefficient given Eq. (45) for values of $\epsilon_z < 10^{-4} \text{m}^2\text{s}^{-1}$ and equal to $10^{-4} \text{m}^2\text{s}^{-1}$ for values greater than $10^{-4} \text{m}^2\text{s}^{-1}$. For the Wellington lake where most major inflows plunge to the bottom of the lake this procedure works very well. However, simulations on Lake Argyle and Kootenay Lake, British Columbia, have shown an intensification of mixing around the inflows. The algorithm is therefore being modified to include intensification of the diffusion coefficient by adding the effects of Eq. (45) and (46). Much more work is required to justify the arbitrary cut-off of $10^{-4} \text{m}^2\text{s}^{-1}$

3.3.2 Turbulent diffusion algorithm. The effective turbulent mixing occurring during a time step is simulated by subroutine DIFUSE, which calculates (separately) the redistribution of salt and heat governed by the diffusion equation. The form of the diffusion equation solved is the constant flux model

$$\frac{\partial y_i}{\partial t} = \frac{1}{\rho_i A_i} \frac{\partial}{\partial z} \left(A_i \rho_i \epsilon \frac{\partial y_i}{\partial z} \right) \quad i = 1, NS \quad (47)$$

when y_i is the property (temperature or salinity), ρ_i the density, and A_i the area of the i^{th} layer. The eddy diffusivity $\epsilon(z)$ is calculated from Eq. (45). This equation is solved explicitly in time steps of one quarter hour, time stepping until the current time step set by HEATR is reached. The entire term on the right hand side, including $\epsilon(z)$ is calculated by subroutine FCT for each layer.

The algorithm introduces a mixing time scale

$$T_M = \frac{E}{P_S + P_W} \quad (48)$$

where E is the potential energy locked in the stratification.

$$E = g \left\{ \rho_{av} \sum_{i=1}^{NS} V_i d_i - \sum_{i=1}^{NS} \rho_i V_i d_i \right\} \quad (49)$$

and P_S and P_W are the rates of working of the inflows and wind respectively

$$P_S = g \Delta\rho D Q \quad (50)$$

for each stream, and

$$P_W = C A_{NS} U_3 \quad (51)$$

with ρ_{av} the average density, V_i the volume and d_i the height of the i^{th} layer, $\Delta\rho$, D and Q the density jump, the level of neutral buoyancy, the river discharge (computed in this instance without entrainment), U the average wind speed, and C a parameter which incorporates the drag coefficient and a factor representing the degree of sheltering of the surface from wind.

Subroutine FCT is called with this value of T_M , the eddy diffusivity is computed, the molecular value for heat is added, and the remainder of the right hand side is evaluated for each layer. The redistribution of salt during one quarter hour period is evaluated by DIFUSE, which ensures that no reversals in gradient occur, the time counter checked against the current time step and the process repeated if necessary. The entire process is then repeated for temperature.

Following these diffusion calculations, the service subroutine THICK is called to split the completely mixed upper layers into a number of smaller layers in anticipation of the next action, either further heat transfer with HEATR or the inflow computations with INFLOW.

3.4 Inflow Dynamics

3.4.1 Theoretical background. The inflow process may be divided into three stages as shown in Fig. 3.3 As the stream enters the lake it will push the stagnant lake water ahead of itself until buoyancy forces, due to any density differences which may be present, have become sufficient to arrest the inflow. At this point the flow either floats over the reservoir surface if the inflow is lighter or it plunges beneath the reservoir water if it is heavier. If the entrance point is a well defined drowned river valley, as in most reservoirs, then the side of the valley will confine the flow and a plunge line will be visible across the reservoir at which point the river water submerges uniformly and travels down the channel in a one-dimensional fashion.

Once the inflowing river has negotiated the plunge line it will continue to flow down the river channel, entraining reservoir water as it moves towards the dam wall. Hebbert *et al.* (1979), generalizing the work of Ellison and Turner (1959), show that the entrainment coefficient E is given by

$$E = - \frac{h}{2u\Delta} \frac{D\Delta}{Dt} \quad (52)$$

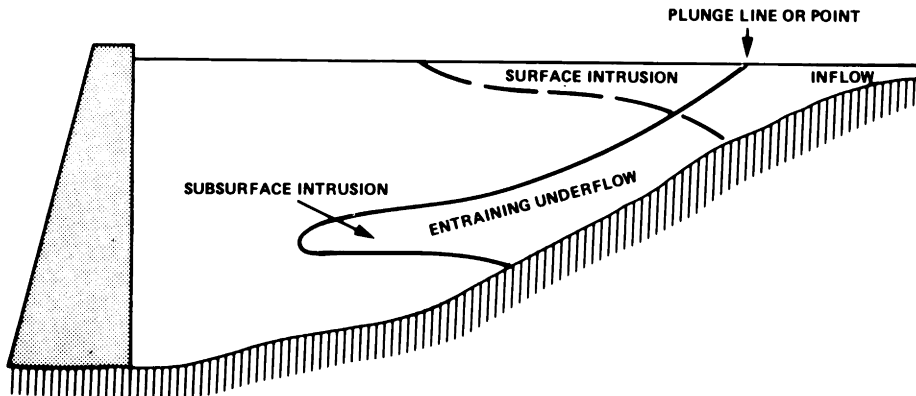


Figure 3.3. Schematic of the various inflow configurations parameterized in DYRESM.

in which Δ is the non-dimensional density anomaly $\Delta = (\rho_u - \rho_r)/\rho_r$, ρ_u and ρ_r the underflow and reservoir densities, u the mean velocity of the underflow, and $D\Delta/Dt$ the variation in Δ moving with the mean velocity u . Direct measurements of u , Δ and h yielded a value of $E = 1.9 \times 10^{-4}$ for the Collie River Valley.

By assuming that the discharge varies slowly in comparison to the internal adjustment time, and the valley section was approximately triangular, Hebbert *et al.* (1979) showed that the drag coefficient may be expressed as

$$C_D = \frac{\sin\alpha}{5} \left(\frac{5\sin\Phi}{F_i^2} - \frac{4}{3} E \left\{ 3 + \frac{2}{F_i^2} \right\} \right) \quad (53)$$

where F_i is the internal Froude number, $F_i = u/(gh)^{1/2}$, h is the hydraulic depth, and Φ the angle between the river bed and the horizontal. For normal flow, F_i is constant. With the above value of E , $\tan\Phi = 10^{-3}$, and $F_i = 0.24$, Eq. (52) implies a value of $C_D = 0.015$ for the Collie River Valley.

The corresponding Manning's n is 0.05, which is typical for such a natural stream.

Rewriting Eq. (53) for the entrainment E yields

$$E = \frac{3}{4} \left\{ \frac{5\tan\Phi}{F_i^2} - \frac{5C_D}{\sin\alpha} \right\} \frac{F_i^2}{(3F_i^2 + 2)} \quad (54)$$

where F_i is determined by the slope and roughness of the river bed. The corresponding expression for the flowing depth h then follows. (See Hebbert *et al.*, 1979).

Little data exist about the relationship between F_i , the slope of the bed and the bed roughness. The dynamics of the underflow are however characterized by the same processes as those described for the mixed layer and the TKE Eq. (27) may be applied here. For streams with very mild slopes all the entrainment will be

induced by the bottom shear stress u^* , where

$$u^* = C_D^{1/2} u$$

Now since F_i is small, $C_T = 0$, and $w^* = 0$, Eq. (27) reduces to

$$E = \frac{\eta^3 C_k C_D^{3/2} F_i^2}{2} \quad (55)$$

On first thought $\eta^3 C_K$ should be the same as found for the mixed layer dynamics. However, the experiments of Hebbert, *et al.*, (1979) and Elder and Wunderlich (1972) suggest a considerably higher efficiency of 3.2 for mixing in a downflow. The difference is most probably due to the very different distribution of mean shear within the underflow.

Equating Eqs. (54) and (55) leads to the result

$$F_i^2 = \frac{\sin\alpha \tan\Phi}{C_D} (1 - 0.85 C_D^{1/2} \sin\alpha) \quad (56)$$

Hence, once C_D is fixed F_i and E , can be determined.

The entrainment E leads to an increase ΔQ in the underflow volume Q given by conservation of volume

$$\Delta Q = Q \left(\left\{ \frac{h}{h_o} \right\}^{5/3} - 1 \right) \quad (57)$$

The flow may thus be routed down the river channel of a stratified reservoir by assuming the flow to be gradually varied and by applying Eqs. (54), (56) and (57) locally in each horizontal slab within which the density is assumed constant. At the transition from one slab to the next h_o is redefined so that Q and F_i are continuous across the transition. In this way the flow may be routed down the channel slope until neutral conditions are achieved, at which stage the horizontal penetration of the slug is assumed to commence.

To start the algorithm the initial h_o is required from a plunge point analysis. For a triangular cross section, Hebbert *et al.*, (1979) equated Eq. (56) to the entrance Froude number and showed that the initial flowing depth h_o is given by

$$h_o = \left\{ \frac{2Q^2}{F_i g \Delta \tan^2 \alpha} \right\}^{1/5} \quad (58)$$

This formulation applies only for streams of small bed slope; in the case of larger bed slopes, shear production and mixing at the plunge point must also be considered.

The entrainment given by Eq. (55) leads to a decrease in the density of the plunging inflow until at some level, the inflow and reservoir densities balance and the inflow penetrates the reservoir. This intrusion into a stratified water body has been studied by Imberger *et al.*, (1976) and is characterized by the non-dimensional number $R = F_i Gr^{1/3}$, where Gr is the Grashof number $N^2 L^2 / \epsilon_z^2$ and F_i is the Froude number BNL^2 / Q , both being determined at the point of insertion. The length of the intrusion e is given by

$$e = 0.44 LR^{1/2} t' \quad t' \leq R \quad (59)$$

$$e = 0.57 LR^{2/3} (t')^{5/6} \quad R < t' \leq Pr^{5/6} \quad (60)$$

where $t' = tN/Gr^{1/6}$, Pr is the Prandtl number of the fluid, N the Brunt-Vaisala frequency and L the reservoir length at the level of insertion. Equation (59) describes an inertia-buoyancy balance and Eq. (60) a viscous-buoyancy balance. For $R \geq 1$ Eq. (59) is valid for the whole intrusion process; on the other hand, the smaller the value of R , the larger the applicability of Eq. (60). In the context of DYRESM, the process is split at $R = 1$, using Eq. (59) for $R \geq 1$, and Eq. (60) for $R < 1$, irrespective of the time of insertion. Given the two preceding expressions for the length of the intrusion as a function of time it is possible to compute an entrance thickness 2δ such that the inserted fluid is always in “static” equilibrium with the fluid in the slabs which it pushes ahead of itself. Thus

$$\delta = \frac{Q}{B} \left\{ 1 - \frac{e}{L} \right\} \quad (61)$$

in which B is the width at the entrance. The flow to be inserted during one day is then distributed over a thickness, 2δ , such that

$$u = u_{\max} \left\{ \cos \frac{\pi Z}{\delta} + 1 \right\} \quad (62)$$

3.4.2 Inflow dynamics algorithm. The dynamics of the river discharges entering the main body of the reservoir are modeled by the subroutine INFLOW, which is based on the equations described above. The subroutine is called separately for each river entering the reservoir.

The entrance of the river inflow into the reservoir is modeled by the

insertion of the volume into a number of existing layers at the appropriate height. If the layer volumes become excessive, new layers are formed. The increased volume of these layers causes those above to move upwards, decreasing their thickness in accordance with the given volume-depth relationship, to accommodate the volume increase. The layers affected by inflow are those encompassed by the inflow layer thickness 2δ , centered at the level of neutral buoyancy. This level is determined by a comparison of the inflow density, modified by the entrainment from the layers already passed, with the current layer density. The apportionment of the total inflow volume (discharge + entrainment) is done in such a way that the inflow velocity takes a bell shaped profile.

In detail, the computational procedure is as follows. The inflow properties of volume Q , temperature T , salinity s , and density ρ are initialized to the river values. The inflow density ρ is compared with that of the top layer ρ_{NS} : if $\rho < \rho_{NS}$, or $NS = 1$, the total volume is added to the top layer, a new surface level and properties are computed, and the control is returned to the main program. If, however, $\rho > \rho_{NS}$, $NS \neq 1$, and underflow occurs, entrainment calculations are necessary.

The entrainment ΔQ from the layers adjacent to the underflow is computed from Eq. (55) and this quantity of water is added to the inflow volume Q . The properties T , S and ρ are then adjusted and ρ is compared with the next lowest layer. If the inflow density is the smaller, the level of insertion is taken to be the mid-point of current layer. If not, the process is repeated until a neutrally buoyant level is found or the bottom is reached. The intrusion layer thickness 2δ is calculated from Eq. (61), and the layer numbers n_B and n_T corresponding to the upper and lower limits of 2δ , centered on the level of insertion, are evaluated.

In the calculation of δ , an iterative procedure ensures that δ is less than the distance over which $d\rho/dz$ is calculated. Thus local density inequalities are prevented from yielding erroneously high δ values.

The total inflow volume is apportioned amongst layers n_B to n_T so that the required velocity profile is achieved. Since the inflow layer may not be precisely symmetric because of the differing model layer thicknesses or intersection of the inflow layer with the surface or bottom, upper and lower thicknesses δ_T , δ_B are formed. Thus the bell shaped profile becomes

$$\begin{aligned} u &= \frac{u_{\max}}{2} \left[\cos \left(\frac{\pi z}{\delta_B} \right) + 1 \right] & z \leq 1 \\ &= \frac{u_{\max}}{2} \left[\cos \frac{\pi z}{\delta_T} + 1 \right] & z > 1 \end{aligned} \quad (63)$$

where z is measured from the level of insertion. Since

$$\int_{-\delta_B}^{\delta_T} u \, dz = q; \quad u_{\max} = \frac{2q}{\delta_T + \delta_B} \quad (64)$$

and the volume inserted into layer i , above the level of insertion is

$$dV_i = \frac{q}{\delta_T + \delta_B} \left[\frac{\delta_T}{\pi} \left(\sin \frac{\pi}{\delta_T} (d_i - d_p) - \sin \frac{\pi}{\delta_T} (d_{i-1} - d_p) \right) + d_i - d_{i-1} \right] \quad (65)$$

A similar expression is obtained for layers below the level of insertion.

3.5 Outflow Dynamics

3.5.1 Theoretical background. The outflow structures of a reservoir vary greatly and range from flow over a sharp crested spillway extending the whole width of the dam to single pipe inlets housed in an offtake tower situated in the central basin. Once again the single pipe outlets differ greatly in design from one lake to the next. However, there are basically two extreme idealizations of these structures which serve as suitable models for the development of the theory. First, the flow may be assumed to be two-dimensional and flowing into a line sink. Second, single pipe outlets may be approximated by point sinks in the stratified lake.

In both cases the flow is determined primarily by the discharge q (or Q for the three-dimensional flow) and the stratification gradient. During peak flows and periods of weak stratification the inertia forces associated with the outflows will be much larger than the buoyancy forces and the flow will not "feel" the stratification. Near the sink the flow will be radial with a potential flow dictated by the geometry in the remainder of the lake (Fig. 3.4a). Such flows are rare, since in most cases the stratification is severe enough to have a first order influence on the flow.

Consider now the extreme of very severe continuous stratification and a small discharge. In this case vertical motion is inhibited, but not horizontal motions or streamline curvatures. The flow under such conditions will be more as sketched in Fig. 3.4b with the fluid below the offtake remaining unaffected by the outflow and the fluid above the outlet falling vertically to make up the volume lost through the outflow but preserving the horizontal isopycnals.

In the potential flow shown in Fig. 3.4a the streamlines are such that the whole depth of reservoir is sampled equally. On the other hand with stratification dominating, the flow becomes selective and the quality of the water withdrawn is the average of an elongated volume extending a long way into the reservoir (Fig. 3.4b).

Often the stratification is not uniform, but characterized by a uniform epilimnion, a very strong pycnocline and only rather weak stratification in the hypolimnion. Withdrawal from an outlet in the hypolimnion (or the epilimnion) leads to three possible flows. First, for small discharges the density gradient in the hypolimnion is sufficient to constrain the vertical motion and the flow is selective. Second, at slightly larger discharges the hypolimnion density gradient is insufficient to prevent drawdown, but the density gradient at the pycnocline inhibits relative

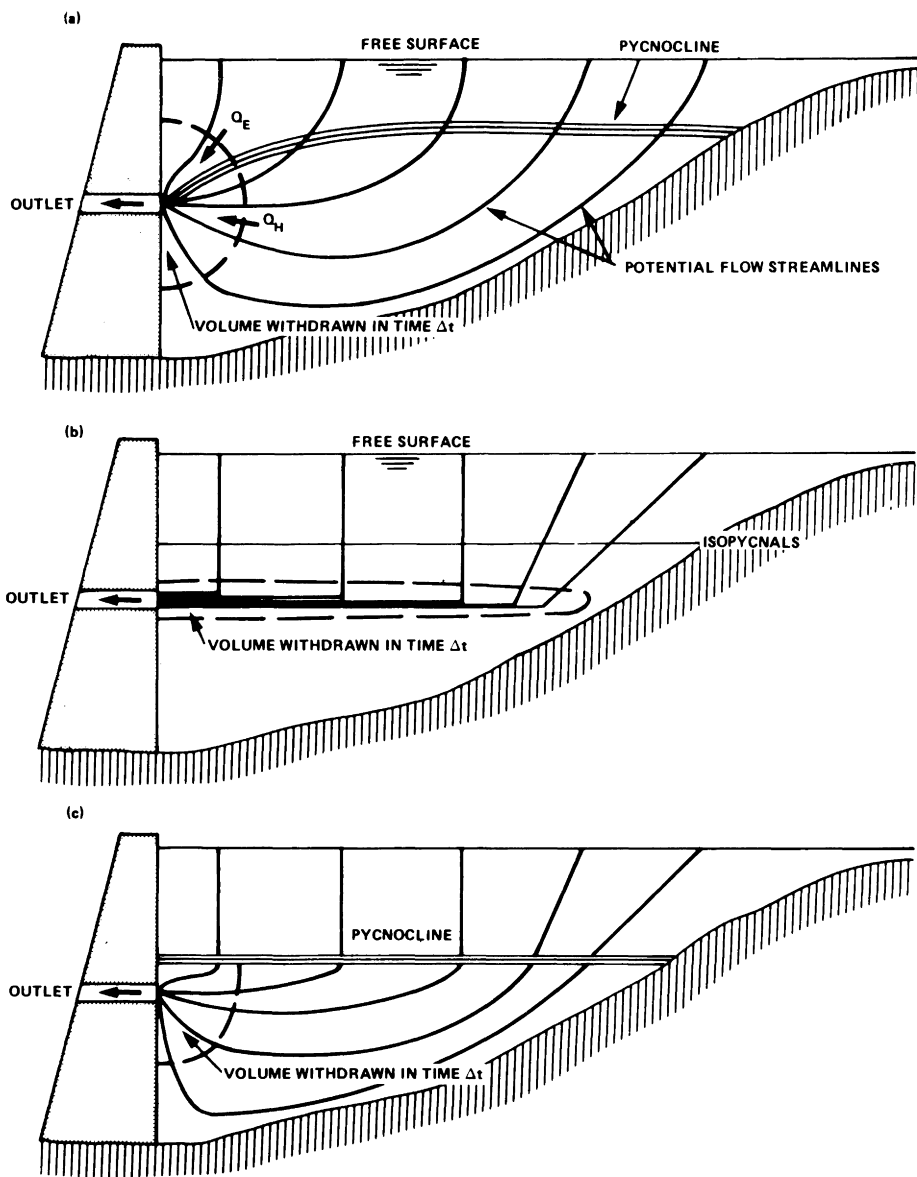


Figure 3.4. (a) Potential flow out through a strong discharge. (b) Selective withdrawal under very stable conditions. (c) Influence of a strong pycnocline on the outflow streamlines.

vertical motion and the pycnocline acts as the free surface in the first case. The water in the epilimnion once again is that in a container with a falling bottom (Fig. 3.4c). Third, as the discharge is raised to a critical value, the pycnocline will also be drawn down (or up for an outlet in the epilimnion) and the water withdrawn will be a mixture of epilimnion and hypolimnion water. The ratio of the mixture will tend increasing to that given by the potential flow solution (Fig. 3.4a) as the discharge is increased or the density difference across the pycnocline is decreased.

In practice, the density profile is as shown in Fig. 3.5. There is usually a well mixed layer containing a diurnal thermocline, a strong pycnocline and a hypolimnion stabilized with a definite density gradient. For weak outlet discharges, the linear stratification model is most applicable, but as the discharge is increased care must be taken that no contradiction arises between the application of this theory and the possibility of drawdown of the seasonal pycnocline. A complete review of the problems has recently been given by Imberger (1980) and we shall confine ourselves to a summary of the applicable formulae.

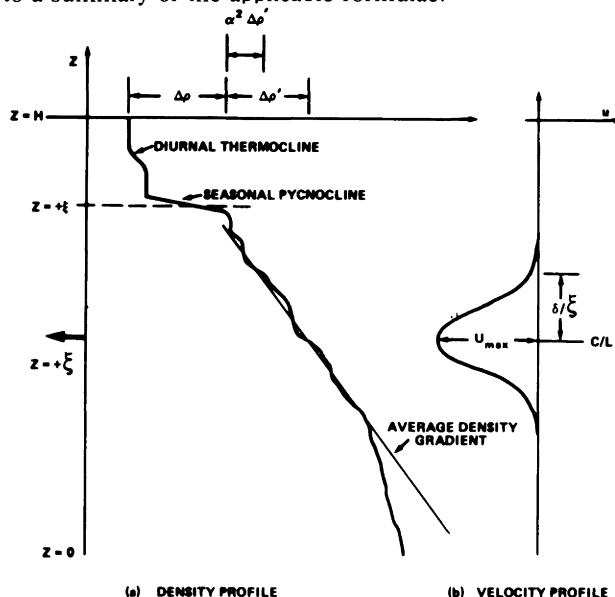


Figure 3.5. Definition sketch of the density and velocity profiles for the selective withdrawal calculations.

Consider first slot outlets, spillway flow or point outlets in very narrow reservoirs.

Let q be the discharge per unit width, N the average buoyancy frequency over the layer thickness, ϵ_z the effective vertical diffusion coefficient, L the length of the reservoir and

$$R_L = F_L Gr_L^{1/3} \quad (66)$$

where $F_L = \frac{NL^2}{q}$ and $Gr = N^2 L^4 / \epsilon_z^2$ then

$$\delta = 5.5 L Gr_L^{-1/6}; \quad R_L < 1 \quad (67)$$

with 64% of the layer lying above the sink centerline and

$$\delta = 4.0 L F_L^{1/2}; \quad R_L > 1 \quad (68)$$

The set up time for these two steady state solutions is $T_L = 0(N^{-1}Gr_L^{1/6})$ for $R_L < 1$ and $T_L = 0(N^{-1}F_L^{-1/2})$ for $R_L > 1$.

The velocity distribution associated with these flows is a complex integral of the equations of motion. However, a good approximation is again given by the equation

$$u = u_{\max} \left(1 + \cos \frac{2\pi z}{\delta} \right) \quad (69)$$

This neglects the weak back flow regions at the boundaries of the withdrawal layers, but in terms of a water quality model this is insignificant as these flows are internal and do not affect the outflow.

The withdrawal layer will intercept the seasonal pycnocline when $\delta/2 = 0(\xi - \zeta)$. The present versions of DYRESM retains the formulation given by Eqs. (67) and (68) and for large discharges any possible sharp density changes are incorporated into the computation by using the average of N . This is not strictly correct since once the discharge has reached the critical value where the layer intersects the pycnocline, the strong density gradients there inhibit the development of the withdrawal to a far greater degree than is accounted for by the average gradient.

The layer intercepts the pycnocline when

$$q = 0.35 (\zeta - \xi)^{3/2} \left(\frac{\Delta\rho' g}{\rho_o} \right)^{1/2} \quad (70)$$

yet drawdown does not occur until

$$q = 2.6 (\zeta - \xi)^{3/2} \left(\frac{\Delta\rho \alpha^2 \rho'}{\beta} g \right)^{1/2} \quad (71)$$

For the two results to agree as $\Delta\rho \rightarrow 0$ requires $\alpha = 0.13$. The correct procedure thus is to test if a change in formulae is warranted or not.

In the case of $R_L < 1$ and the close proximity of an interface is best handled with the average gradient method. In practice the discharge is rarely larger than that given by Eq. (70). DYRESM makes no allowance for this case other than the average gradient method.

Second, consider the flow into single outlets of a dam wall or offtake structure where the lake is very wide and the outflow is essentially radial in the horizontal plane. We shall quantify this assumption after establishing the present formulae.

For very small discharges, where the withdrawal layer is governed by a viscous buoyancy balance there is no difference to that in the two-dimensional case, although Koh's work (1966) indicates that the layers could be about 20% thicker. For Q large enough for the dynamics to be a balance of buoyancy and inertia leads to a withdrawal layer thickness (Imberger, 1980) of

$$\delta = 1.58 \frac{Q^{1/3}}{N^{1/3}} \quad R_{3,L} > 1 \quad (72)$$

where

$$R_{3,L} = F_{3,L} Gr_{3,L}^{1/2}; \quad F_{3,L} = \frac{Q}{NL^3} \quad \text{and} \quad Gr_{3,L} = \frac{N^2 L^4}{\epsilon_z^2} \quad (73)$$

Hence, once again a critical discharge is reached when the layer intercepts the seasonal pycnocline. This will occur when

$$Q = \tilde{Q}_c = 1.00 (\zeta - \xi)^{5/2} \left[\frac{\Delta\rho' g}{\rho_o} \right]^{1/2} \quad (74)$$

For the case of a sink situated in a dam wall (other cases can be considered) draw-down occurs when

$$Q = Q_c = 2.54 (\zeta - \xi)^{5/2} \left[\frac{\Delta\rho + \alpha^2 \Delta\rho'}{\rho_o} g \right]^{1/2} \quad (75)$$

Once again taking the limit $\Delta\rho \rightarrow 0$ requires $\alpha = 0.80$. For Q much larger than Q_c withdrawal will be dominated by the two layer flow and the ratio of epilimnion to hypolimnion draw can be obtained from the laboratory experiments of Lawrence and Imberger (1979). For value of $Q \sim Q_c$ uncertainty still remains. Version 5 of DYRESM has provisions only for two dimensional withdrawal.

The division between whether a particular flow should be considered to be described by three or two-dimensional formulae may be estimated by comparing the magnitude of the drawdown cone with the reservoir width. Since the drawdown cone is given by approximately $4(\zeta - \xi) = 2\delta$ for a drawdown situation (for very large discharge this may be larger) the three-dimensional drawdown must be checked first. If the cone intersects the edges of the reservoir then the two-dimensional formulae are applied. Offtakes in the corner of the reservoir must of course once again have a corrected Q .

The outflow subroutine, OUTFLOW is presently under review to incorporate three-dimensional flow and the possibility of drawdown. The current version uses Eqs. (67) and (68) by defining an equivalent two-dimensional discharge $q = Q/B$, where B is the width of the reservoir.

3.5.2 Withdrawal dynamics algorithm. The computational strategy is similar to that of the inflow model, with the level of withdrawal being fixed as the level of the current offtake. Thus a withdrawal layer is again constructed from Eqs. (67) and (68), depending on the withdrawal volume q in the daily time step and the stratification at the offtake level. In this case however, the upper and lower half layer thicknesses are computed separately as δ_T and δ_B as the withdrawal layer may be highly unsymmetric if located near the thermocline. In addition, the layers generated by withdrawal from the bottom offtake or by overflow are likely to intersect the reservoir bottom and surface respectively and δ_B and δ_T must therefore be restricted.

Once again the daily flow is apportioned over the model layers encompassed by the withdrawal layer $\delta_T + \delta_B$ in such a way that the same velocity profile results. After checking that this apportionment does not completely empty a model layer, the withdrawal volumes are removed from the affected layers, the layers above moved downward to accommodate the volume change, and the properties (temperature and salinity) of the withdrawal computed. The subroutine then returns control to the main program.

In the computational procedure, the layer numbers corresponding to each offtake are precalculated by subroutine RESINT; the layer number n corresponding to the current offtake is passed to OUTFLOW as an argument. This identifies the offtake, the flow volume Q and the offtake height h . The outflow properties are initialized and Q compared with zero. In the case of no withdrawal, the routine is complete and control is passed back to the main program.

If Q is non zero, the computation of the half layer thicknesses begins, after first checking that more than one model layer is present. If only one layer exists, all the withdrawal is taken from that layer. The calculation of δ_T and δ_B is performed by two passes through a loop. In either case, an iterative procedure is employed to ensure that the calculated δ is smaller than the distance dz over which the local density gradient is calculated, ensuring that local density gradients do not lead to erroneously high δ values. The bounds of the withdrawal layer $h - \delta_B$, $h + \delta_T$ are checked against the reservoir bottom and surface and the δ values changed if necessary.

In order to apportion the total volume Q amongst the layers, the layer numbers i_B, i_T corresponding to the lower and upper bounds of the withdrawal layer are determined. The apportionment of the volume to layers i_B to i_T is identical to the procedure for inflow and the volume taken from the i^{th} layer is given by the same expression. In this case, each dV_i must be checked against the total model layer volume V_i to ensure that a layer is not completely emptied or attains a negative volume. Should this be the case, a small amount is left in the model layer and the remainder of the withdrawal component spread equally over the neighboring layers.

Subject to this adjustment, the dV_i are removed from the affected layers, the layer heights of these and the layers above adjusted to account for the reduced volume, and the properties of the outflow computed as a mixture of the dV_i from the respective model layers. The algorithm is now complete, and control is passed back to the main program.

3.6 Service Subroutines

A number of service routines which are called from the various segments of the main program and the dynamics subroutines complete the structure of DYRESM. These are THICK, which maintains the model layer volumes between specified limits, DENSITY, which calculates the density of water for given temperature and salinity, SATVAP, which evaluates the saturated vapor pressure of air corresponding to a given temperature, and RESINT, which provides an interpolation between depths, volumes and areas from the physical data input. Only brief details of these subroutines are given.

THICK: This subroutine ensures that the model layer volumes are maintained between specific limits and is called after any operation which may have affected layer volumes, with the exception of MIXER, which establishes the mixed layer as a single large layer to facilitate the diffusion computations. THICK is called after these computations to maintain good resolution for the heating and cooling calculations following.

The upper layer volume V_{\max} is set to ensure that adequate resolution is maintained, and the lower limit V_{\min} to ensure that an excessive number of layers is not required. However, V_{\min} must also be sufficiently small to avoid problems of numerical diffusion through a large number of layer amalgamations. A good compromise has proved to be $V_{\min} = S/N$, where S is the capacity of the reservoir and N the maximum number of layers allowed, and $V_{\max} = 4 V_{\min}$.

The routine checks each layer volume against V_{\max} and V_{\min} . Any layer exceeding V_{\max} is split into an appropriate number of smallest layers of identical properties, all layers renumbered, and new positions computed by RESINT. A layer smaller than V_{\min} is amalgamated with its smaller neighbor, and all layers renumbered.

DENSITY: This subroutine evaluates the density ρ of water of temperature T and salinity S according to the formula proposed by Chen and Millero (1977).

The routine is called after any mixing of two layers, or any readjustment of a layer property.

SATVAP: In many cases the surface temperature is not available as daily data. Thus the saturated vapor pressure at the surface temperature, required by HEATR, is not able to be precalculated. Subroutines SATVAP evaluates this variable, using the predicted surface temperature T .

RESINT: Subroutine RESINT calculates the layer volumes and surface areas corresponding to given layer heights or conversely, layer heights and surface areas corresponding to given volumes. The routine is called following any operation which affects either volumes or heights.

In either case the calculation is an interpolation on the given depth-volume-area data for the reservoir, which is assumed to have the local functional form

$$\frac{V_i}{V_{i-1}} = \left[\frac{d_i}{d_{i-1}} \right]^{a_i} \quad (76)$$

$$\frac{A_i}{A_{i-1}} = \left[\frac{d_i}{d_{i-1}} \right]^{b_i} \quad (77)$$

where V_i, A_i and d_i are the i^{th} volume, area, and height data value given.

An additional function of RESINT is to evaluate the model layers corresponding to the levels of the various offtakes and the crest. This is performed by comparing each layer height with the given height of each offtake.

4. DISCUSSION

The development of DYRESM and the associated algorithms described in Section 3 are part of a program designed to understand the physical mixing processes in a lake. The priority attached to the many processes operating in a lake is determined by the long standing aim to obtain a fuller understanding of the interaction between physical mixing processes and the biological kinetics of the lake. The initial construction and constant updating of DYRESM thus serves a twofold purpose. First, it is an organized way to evaluate the influence of a particular process to the overall mixing patterns in a lake, to validate a particular parameterization and to study the competition for available energy among the great host of mixing mechanisms. Second, DYRESM serves as a useful predictive tool for testing reservoir management strategies, for evaluating methods for the control of the lake stratification and for water quality simulations.

DYRESM has been tested on a number of different lakes, but its major evaluation and development has taken place with data from the Wellington Reservoir. This storage is situated about 160 km south of Perth in Western Australia and has a storage capacity of $185 \times 10^6 \text{m}^3$. The reservoir is approximately 30 m

deep at the dam wall, extends some 24 km along the main Collie River Valley and has a surface area of approximately 16 sq. km at the crest level.

The catchment has been severely disturbed by clearing native forest for agricultural development. This has resulted in substantial increases in the stream salinities with the first winter flows possessing salinities as high as 3500 p.p.m. Salinities generally decrease during the late winter and spring. These high salinities, although extremely detrimental to the usefulness of the storage, are valuable for the critical evaluation of the model. In this lake the temperature and the conductivity of the water form two independent tracers with independent inputs.

The seasonal variability of the various inputs to the reservoir over the period from the Julian day 133 in 1975 to day 365 in 1977 are shown in Fig. 4.1a. Depicted are the wind speeds, the short-wave solar radiation as computed from cloud cover records, the salinity and temperature of the inflowing water and the total rate of inflow from the Collie River which contributes approximately 85% of the total inflow. The remaining inflow is included in the simulations, but is not shown in Fig. 4.1a.

Figures 4.1b and 4.1c show the field temperature and salinity structures length averaged along the Collie River Valley as a function of time over the period January 1975 to August 1978. The salinity data gathered between October 1977 and June 1978 is regarded as unreliable and is not shown. The broken lines in Fig. 4.1b indicate that no data was taken in the period covered and the thermal structure is interpreted from the structure before and after the period of interruption.

The yearly cycle is clearly evident in Figures 4.1a and 4.1c. The cold salty inflows lodge in the base of the homogeneous reservoir in the months of June, July and August. Summer stratification builds up until December, when surface winds begin to mix the surface layers and a thermocline forms, protecting the waters below. In early winter, the air temperature falls and the winds increase, with the result that the reservoir is completely mixed before the following inflows arrive. The marked difference in the thermocline structure between 1976 and 1977 was caused by a change in the withdrawal policy. In 1976 all the water was withdrawn from the offtakes at 15 m height, whereas in 1977 a large quantity of salty water was scoured through the offtake at the bottom of the dam wall.

It is also clear from Fig. 4.1b that the temperature regime of the reservoir is determined by the inflows and the surface heating and cooling. The bottom temperature of the reservoir for most of the year is determined by the temperature of the coldest inflows, whereas the surface temperature is determined by the meteorological forcing. This is typical of lakes in temperate regions, and is in contrast to tropical lakes, where the temperature regime is solely determined by the meteorological inputs.

The data set gathered at the Wellington Reservoir forms an ideal test for DYRESM or any other model. The data was collected at reasonably regular intervals and a series of process oriented field expeditions yielded further data on many of the details of individual events. This work is continuing and it is to be expected that further development of DYRESM will take place from these results.

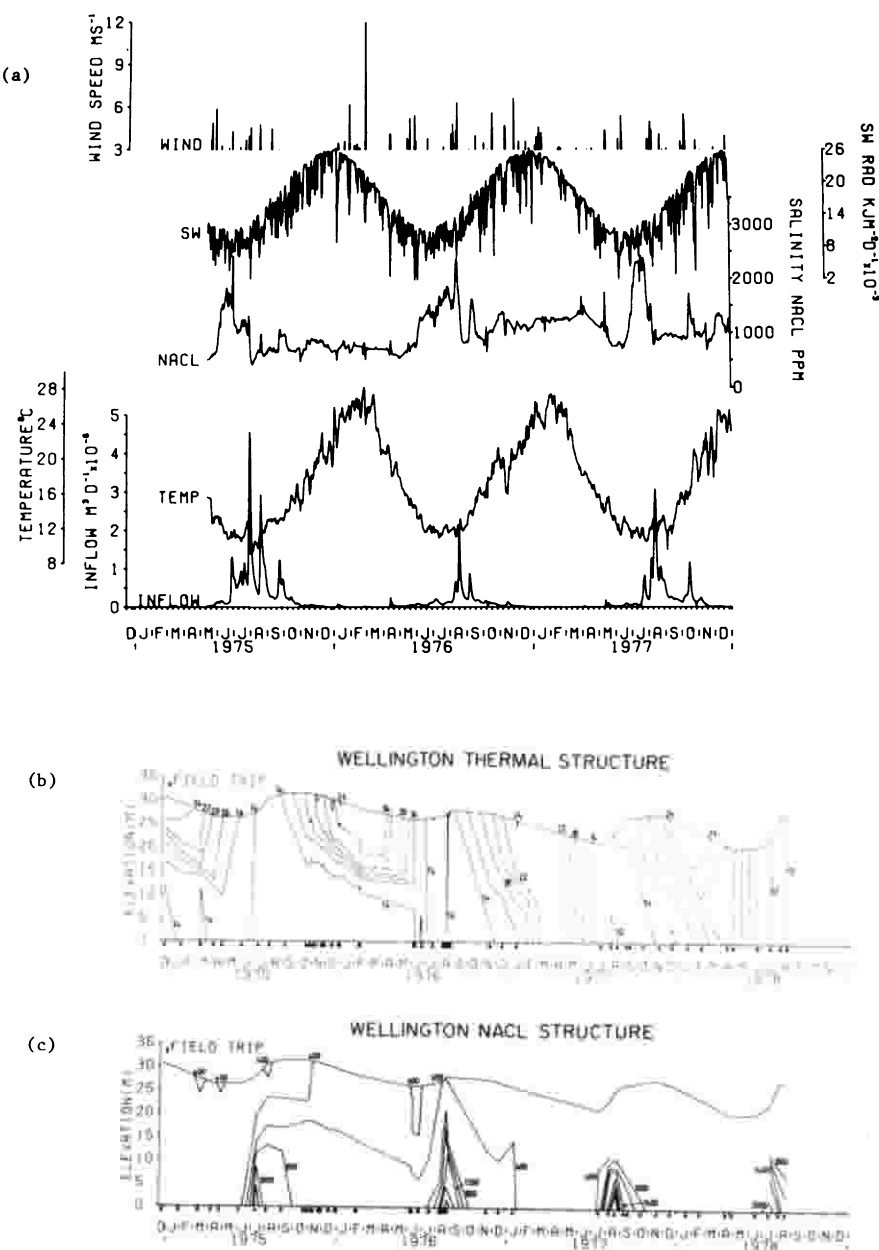


Figure 4.1. (a) Seasonal variation of wind speed, short-wave radiation, salinity and temperature of inflow and discharge for the simulation period of the Wellington Reservoir. (b) Field data showing the temperature structure in the Wellington Reservoir for the duration of the simulation period. (c) Field data showing the salinity structure in the Wellington Reservoir for the duration of the simulation period.

There are seven constants which must be specified by the user before applying DYRESM. Of these only one is truly adjustable--the others are related to well identified physical processes and are determined from experimental or field data. The constants are described below, together with experimentally determined values.

1. C_D is the drag coefficient for inflowing streams. C_D was determined independently of DYRESM in a field study described in Hebbert *et al.*, (1978). The value determined in that study, $C_D = 0.015$, is used here.

2. η_1 is an extinction coefficient for short-wave solar radiation penetrating the water. It relates the solar radiation received at the water surface, to that penetrating to a depth z . A single exponential decay formula was used as only limited field measurements were available. An average value of $\eta_1 = 0.35$ is taken from data presented by Hutchinson (1975), based on the fact that the Wellington is fairly clear in the summer months when surface heating is an important effect.

3. α_1 is a constant occurring in the expression for the diffusivity calculated for the deep hypolimnetic mixing. It represents the efficiency with which the power input from the surface wind and river inflows is converted to a gain in potential energy of the lake water due to vertical mixing. A value $\alpha_1 = 0.048$ determined in earlier calibrations of DYRESM over the 100 day period from day 133 to 233 has proven satisfactory throughout.

4. C_K is the coefficient measuring the stirring efficiency of convective overturn. Experimental results summarized by Fischer *et al.*, (1979) suggest an average value of $C_K = 0.125$.

5. η , in combination with C_K as $C_K \eta^3$, is a coefficient measuring the stirring efficiency of the wind. The value given by Wu (1973) is adopted here, since it was shown by Spigel (1978) that in his experiments stirring effects dominated the entrainment, with shear production, temporal effects, and internal wave radiation losses negligible. Wu's deepening law is $dh/dt = 0.23 u^*/Ri^*$ giving $C_K \eta^3$, and thus $\eta = 1.23$.

6. C_S is the coefficient measuring the efficiency of shear production for entrainment. Values ranging from 0.2 to 1 are reported by Sherman *et al.*, (1978). $C_S = 0.2$ was chosen as representing a good estimate for most experimental results. A value of 0.5 was used before the energy released by billowing was separately included as is done in version 5 of DYRESM.

7. C_T is associated with temporal, or unsteady, non-equilibrium effects due to changes in surface wind stress or surface cooling. C_T is constructed by the requirement that for a turbulent front entraining into a homogeneous fluid, $dh/dt = 0.3u^*$ (Zenman and Tennekes, 1977) giving a value of $C_T = C_K \eta/0.3 = 0.510$.

These coefficient values were used for a 962 day simulation of the lake dynamics starting with initial profile data on day 75133. The results from this simulation are shown in Figs. 4.2a and 4.2b.

Comparison of Figs. 4.1b and 4.2a shows that the thermal structure is reproduced extremely well with all the stratifying and mixing regimes occurring at the

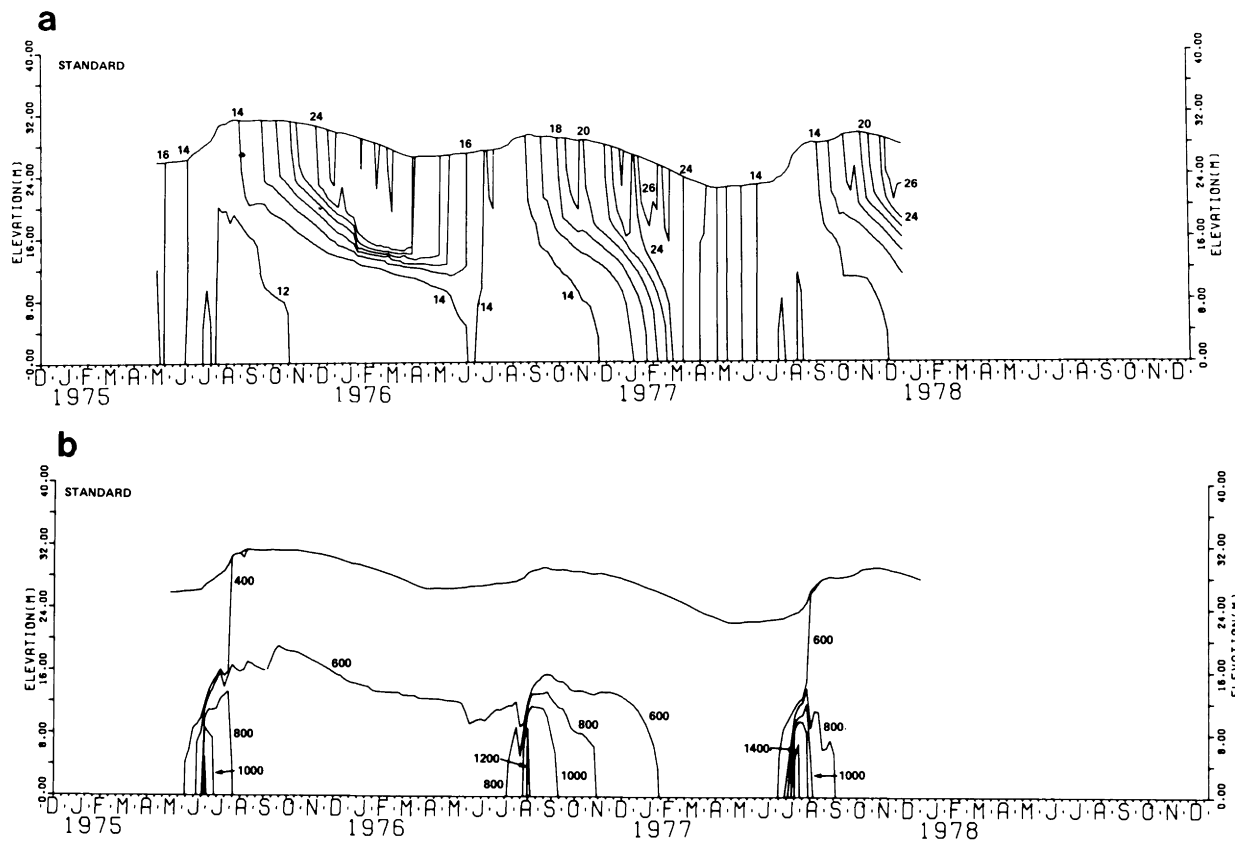


Figure 4.2. (a) Simulated temperature structure (compare to Fig. 4.1b). (b) Simulated salinity structure (compare to Fig. 4.1c).

correct times and of the correct magnitude. The slug of 12°C water predicted by the model in August to September 1975 does not appear in the field data. This slug is derived from the previous inflow and its presence may be due to errors in the inflow temperature data. In any case, the predicted temperature gradient in the bottom at this time is small, and the actual difference between field and predicted temperatures is less than 1°C.

The predicted and observed salinity variations also compare well, the most significant anomaly being the mismatch of the 600 p.p.m. line at the period of maximum inflow in 1976. The field data suggest somewhat more energetic surface mixing which may be due to small errors in the wind data. Additionally, the model does not reproduce the peak salinities of the inflows. This is due to the construction of the model layers in terms of layer volumes, hence fixed by the depth resolution in the upper part. The bottom three or four meters always appear as mixed, and any salinity slug occupying less than this will be mixed with the layer above. Thus, there is no error in terms of the salt load, but one of display of the structure, and it was accepted in order to save computer time. If greater resolution were required, this could be achieved by specifying smaller minimum slab sizes.

Overall, DYRESM appears to faithfully reproduce even very severe changes in the reservoir structure caused by such diverse forcing as large saline inflows, active scouring, strong wind deepening and winter convective cooling. Perhaps more importantly, the model correctly simulates two independent parameters, salinity and temperature, to a resolution equal to that of the field program. More accurate field data is required if more stringent tests are to be applied.

Profile data, as computed by the various components of MIXER are reproduced in Fig. 4.3 for day 75138. The result of each computational step is shown starting with Fig. 4.3a which depicts the result of HEATR adding both the surface heat losses and the subsurface heating due to solar radiation penetrating to some depth. A 3°C deficit due to surface cooling, was quickly achieved, leaving a convectively unstable density profile, Fig. 4.3b, with a density anomaly of nearly 0.5 kg m^{-3} . The potential energy stored in this unstable profile is released by relaxing the density profile until it and the mixed layer have reached a depth of 5 meters. The total amount of potential energy released yields the effective convective velocity scale w^* (Fig. 3.4c). The stirring energy $C_K/2\eta^3 u^{*3} \Delta t$ is then added to this pool of TKE causing a further deepening of the mixed layer of 3.6 meters (Fig. 3.4d). The velocity in the mixed layer is reduced due to the deepening, but there is still sufficient mean kinetic energy to cause further 2 meters of deepening by shear production as is seen in Fig. 3.4e. At this stage the algorithm leaves a structure characterized by a mixed layer and a sharp thermocline. The subroutine K-H smears this interface over a distance $0.3 \Delta u^2/g'$ which in this case amounted to nearly 3 meters (Fig. 4.3f). This process is carried forward from one time step to the next.

On day 75138 all the deepening processes were additive. This is not always the case as is illustrated by the deepening on day 75228. In Fig. 4.4a the net surface heat flux is plotted as a function of time and in Fig. 4.4b the corresponding ΔU (final) for the mixed layer. The plot in Fig. 4.4c shows the resulting mixed

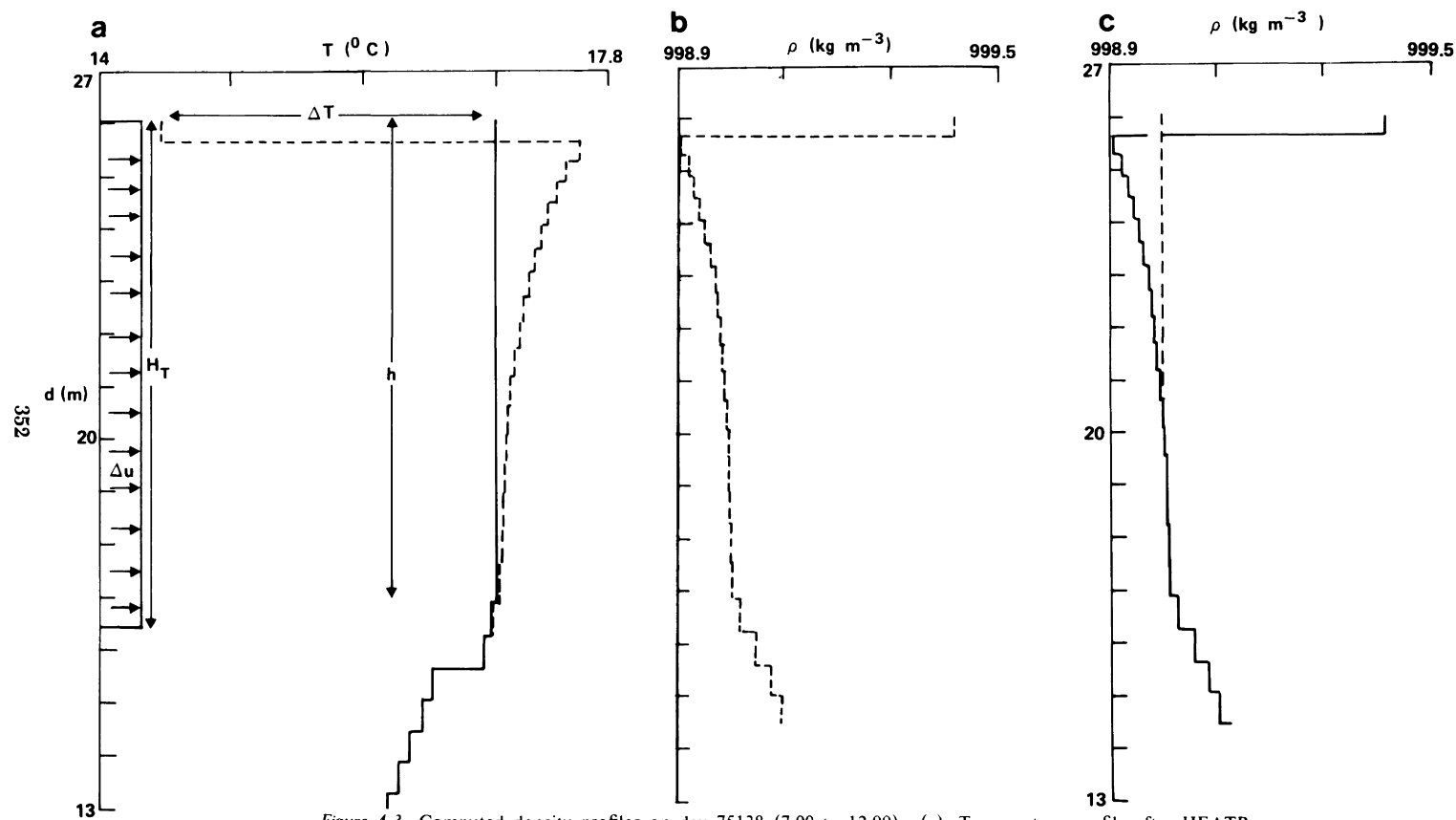


Figure 4.3. Computed density profiles on day 75138 (7.00 to 12.00). (a) Temperature profile after HEATR.
(b) Density profile after HEATR. (c) Density profile after convective overturn has stabilized profile.

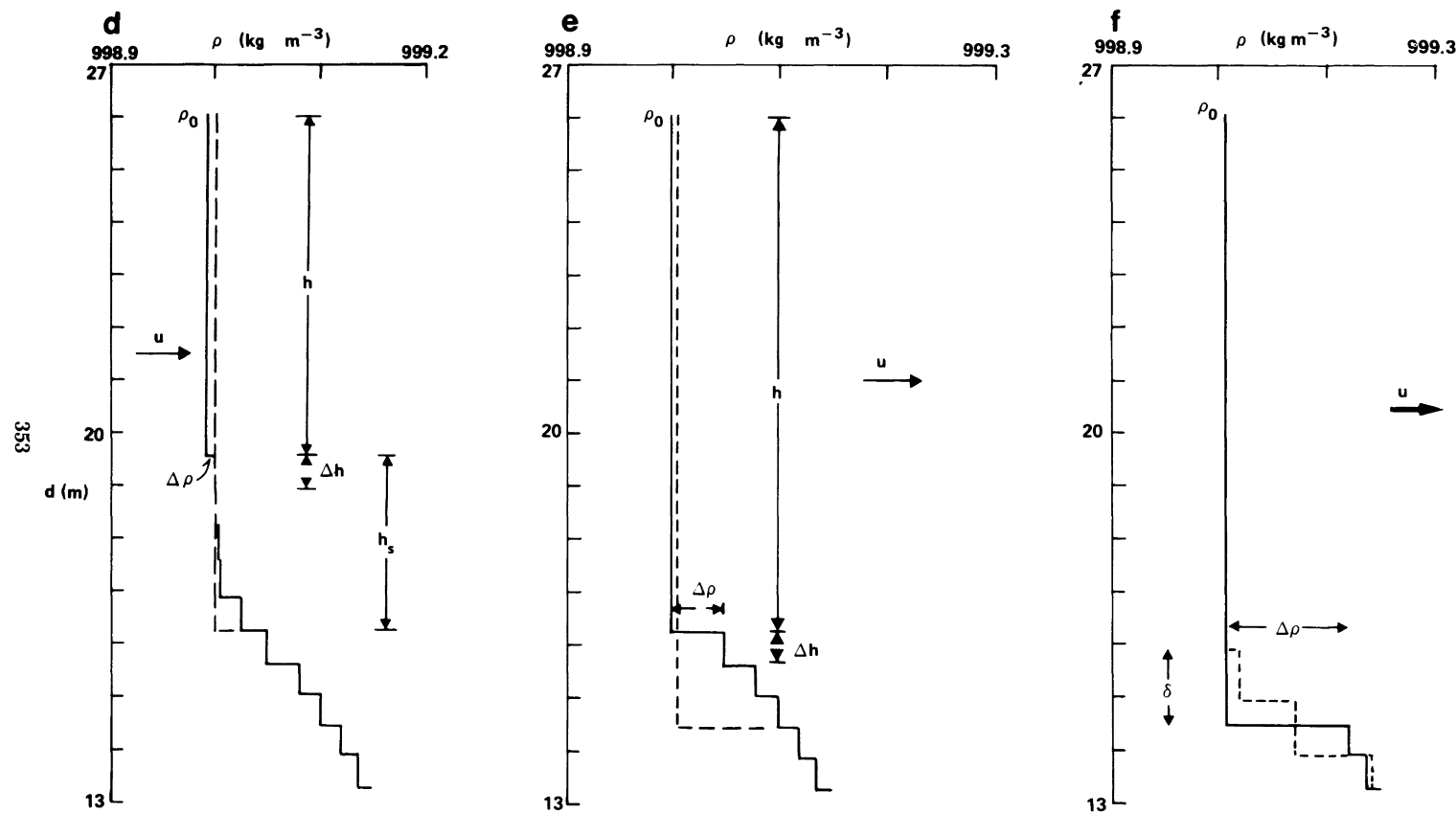


Figure 4.3, continued. (d) Density profile showing deepening due to surface energy inputs. (e) Deepening due to shear production. (f) Smearing of the pycnocline due to K-H billowing.

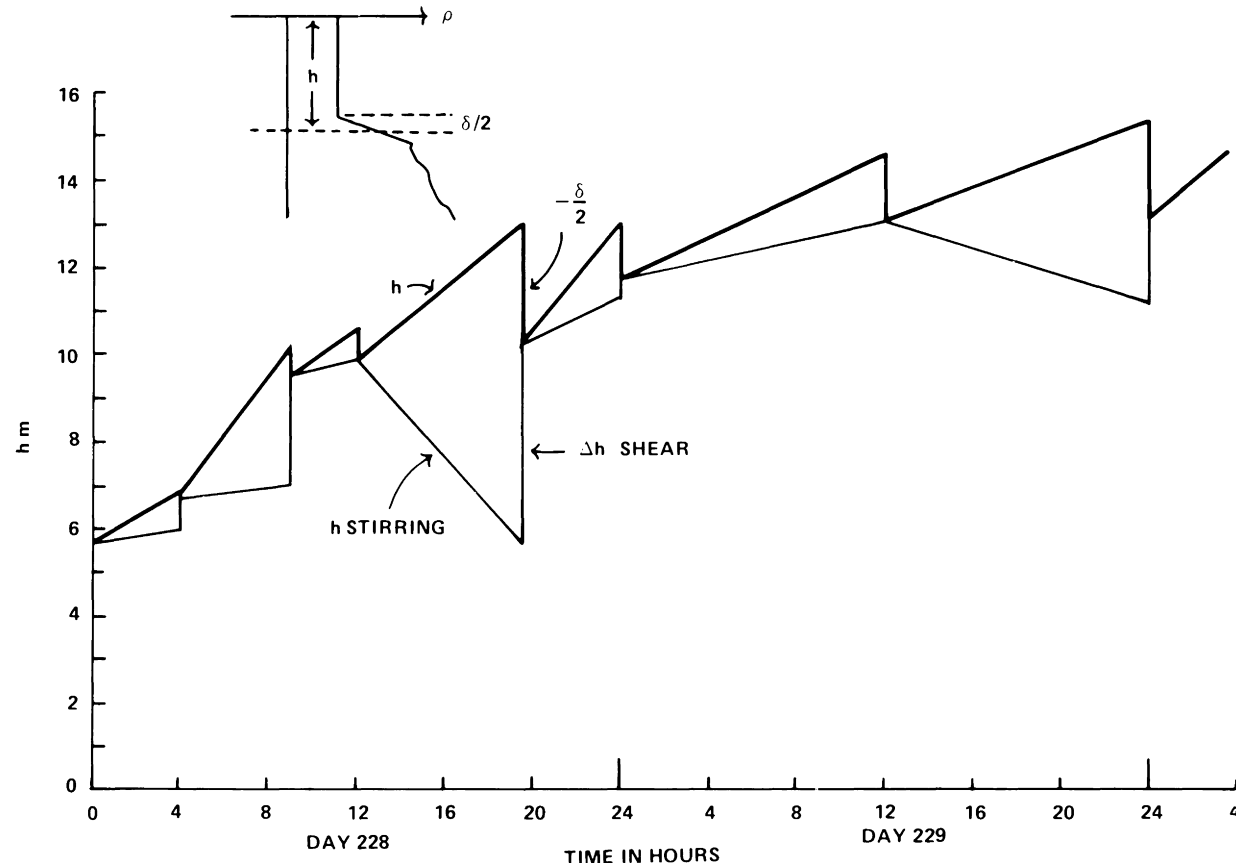


Figure 4.4. Deepening predictions on day 75228. (a) Thermal input at the surface. (b) Calculated mean speed of mixed layer. (c) Predicted deepening. Solid line is net depth of mixed layer. Thin line represents deepening only due to the stirring mechanism. Jumps at each time step account for K-H billowing. Notice the decrease in the depth during the 4th time step if only stirring energy is accounted for.

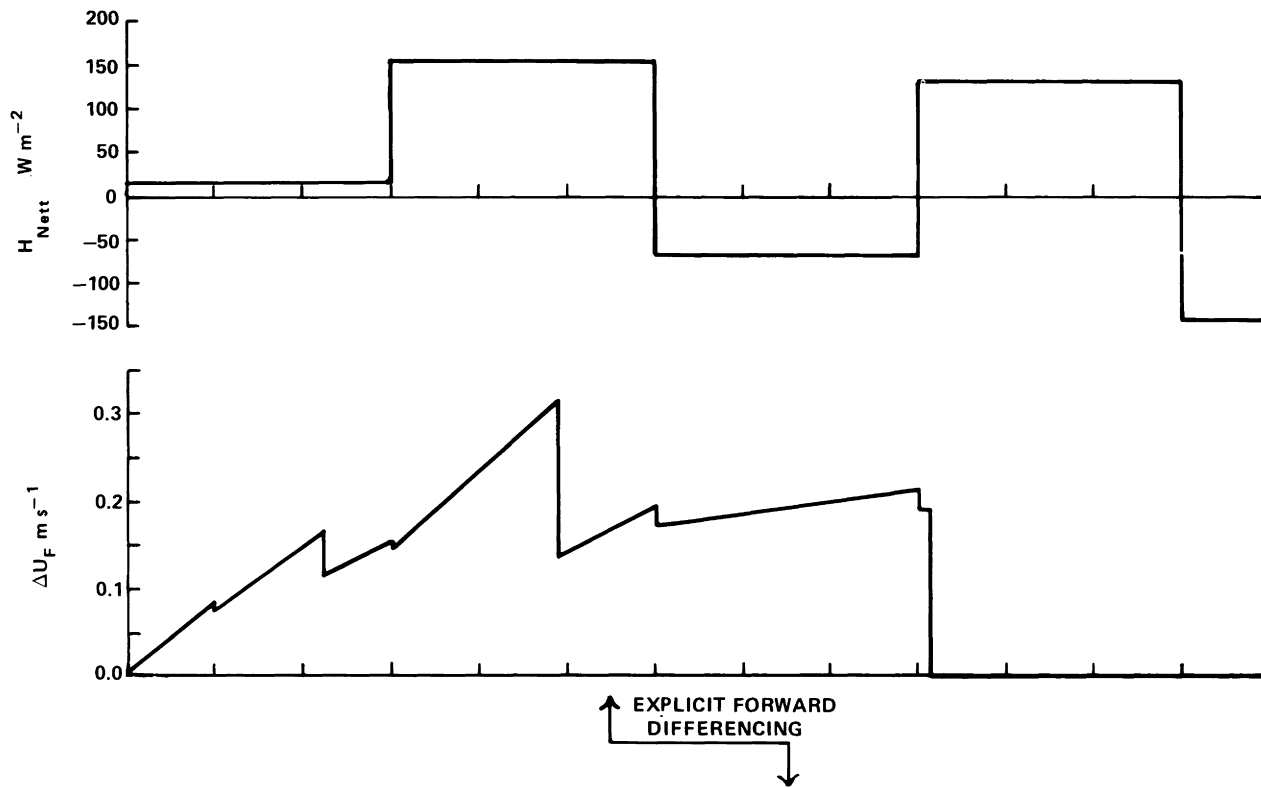


Figure 4.4, continued.

layer behavior. The solid line is the total depth after all the processes illustrated in Fig. 4.3 have acted. The thin line shows the deepening due to stirring only and the jump at the end of each time period is the result of K-H billowing decreasing the layer depth. In the fourth time period, at the beginning of severe surface heating the stirring mechanism actually predicted a decrease in layer thickness. This is explained simply by noting that the Monin-Obukhov length was decreased by the positive buoyancy flux due to the surface heating. The decreased depth however raised the velocity and greatly enhanced shear deepening.

Each day of the simulation is a variation of these two extremes and the depth of the mixed layer at the end of a season is merely the cumulative effect of individual diurnal deepening events.

The subroutine DIFUSE is called after the mixed layer dynamics calculations have been completed. Fig. 4.5 is a graph of the density profile of day 75138 and the associated vertical diffusion coefficient for heat. The value of $10^{-4} \text{ m sec}^{-1}$ is the cut-off value introduced to simulate a fully turbulent condition. It is seen that as N increases ϵ_z decreases sharply leading to decreased mixing in stable regions.

The great advantage of DYRESM is that each mixing process may be identified and each constant has a well-defined influence on the simulated results. In Fig. 4.6b to 4.6d are shown three perturbations around the standard simulation reproduced in Fig. 4.6a.

First, increasing the shear production efficiency greatly increases the deepening during the wind events in January of 1976, but otherwise introduces little change. The structure recovers quickly from the overdeepening indicating that the dynamics of the Wellington Reservoir are strongly forced with little long term "ringing" of the structure. This is also reflected in the short seiching periods. This is not the case for a recent simulation of Kootenay Lake in British Columbia. Here T_i was close to 28 days and the structure tended to oscillate for long periods after a wind event. This necessitated a modification of MIXER routine which captured the wind direction as well as the wind speed.

The arbitrary cut-off of $10^{-4} \text{ m}^2 \text{ sec}^{-1}$ in the diffusion coefficient has only a minor influence on the temperature structure as is illustrated in Fig. 4.6c where the cut-off has been raised to $10^{-2} \text{ m}^2 \text{ sec}^{-1}$. The salinity concentrations were however, appreciably altered with the increased diffusion reducing the peak salinity at the bottom. These simulations make clear that the diffusion in the hypolimnion is a two parameter process; the second parameter being the appropriate diffusion in the absence of stratification.

The importance of good input data is shown in Fig. 4.6d. A bad data point in February of 1976 was not discovered until the recent introduction of the billowing subroutine. Previous versions of DYRESM were insensitive to isolated short duration wind episodes, but as seen in Fig. 4.6d a 12 m sec^{-1} wind in February now had a dramatic deepening influence. A check of the wind record revealed an error in transcription.

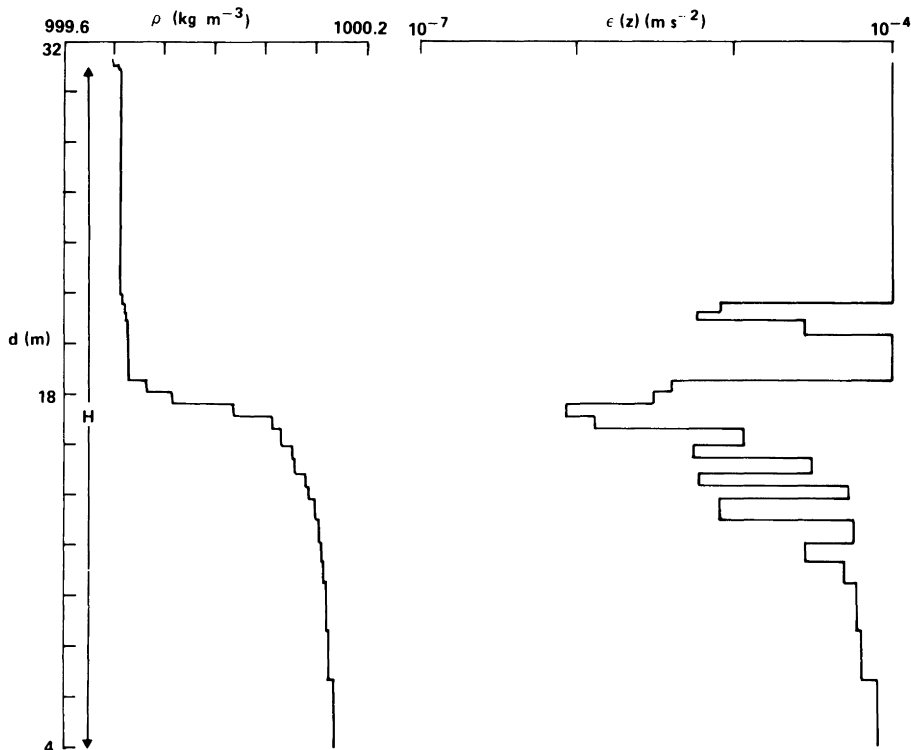


Figure 4.5. A plot of density and vertical diffusivity on day 75138.

5. CONCLUSION

The dynamic simulation model DYRESM appears to successfully model the dynamics of small and medium sized lakes. The model has only one calibratable coefficient and even the value of this is not expected to vary much from one lake to the next. The model has been validated in terms of temperature and salinity variations in 3 major lakes and two lakes with only poor data. It is now necessary to collect data specific to certain processes in the lake and validate the details of the algorithms MIXER and DIFUSE. Such a field program has been commenced in Western Australia.

Certain changes to version 5 are presently in progress. These include the provision for drawdown at the offtake structure, localizing mixing around a river intrusion, the effect of wind direction, a specific parameterization of boundary mixing and the influence of rotation on the shear production parameterization.

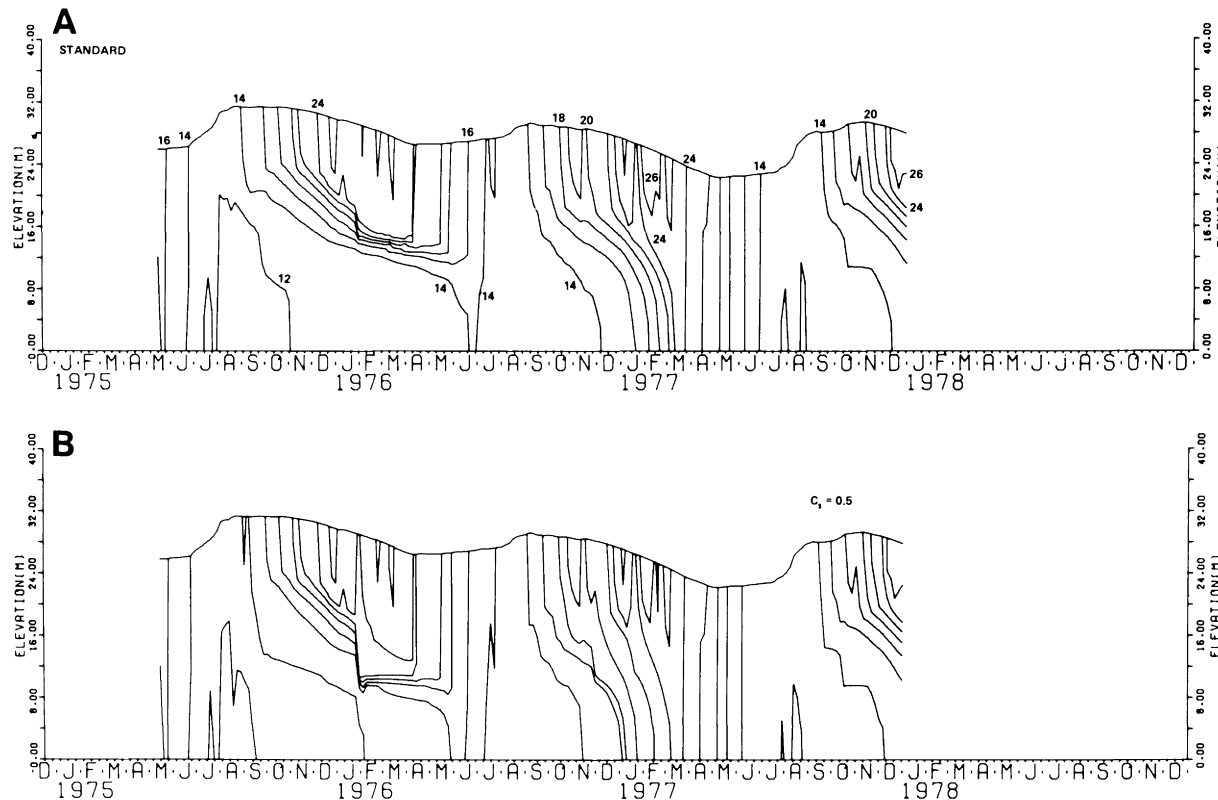


Figure 4.6. (a) Predicted temperature structure. (b) Predicted temperature structure with C_s increased to 0.5

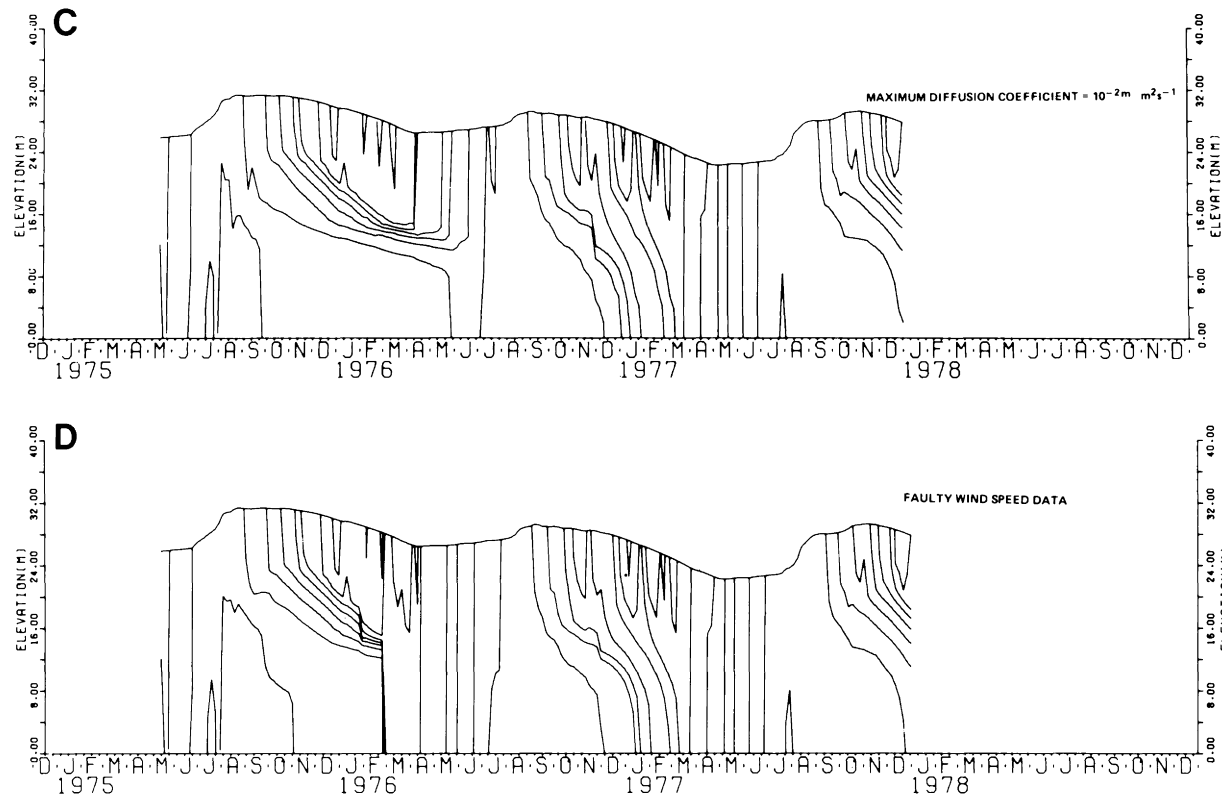


Figure 4.6, Cont. (c) Predicted temperature structure with diffusion coefficient cut-off raised to $10^{-2} \text{ m}^2 \text{ sec}^{-1}$.
(d) Predicted temperature structure showing the influence of an erroneous wind speed of 12 m sec^{-1} in February 1976.

Acknowledgements. DYRESM has been under development for over 6 years and numerous people have contributed to its construction. In particular the authors would like to thank Dr. Robert H. Spigel for his involvement in the MIXER subroutine.

The model was developed with funding from the Australian Water Resources Council, the Water Resources Center of the University California, the Australian Research Grants Committee, the Public Works Department of Western Australia and the Metropolitan Water Supply, Sewerage and Drainage Board of Western Australia. This assistance is gratefully acknowledged.

REFERENCES

- Carson, D. J. and Richards, P. J. R. (1978). Modelling surface turbulent fluxes in stable conditions. *Boundary-Layer Meteorol.* **14**, 67-81.
- Chen, C. T. and Millero, F. J. (1977). The use and misuse of pure water PVT properties for lake waters. *Nature* **266**, 707-708.
- Corcos, G. M. (1979). The Mixing Layer: Deterministic Models of a Turbulent Flow. College of Engineering, University of California, Berkeley, Report No. FM-79-2.
- Corcos, G. M. and Sherman, F. S. (1976). Vorticity concentrations and the dynamics of unstable shear layers. *J. Fluid Mech.* **73**, 241-264.
- Deardorff, J. W. (1968). Dependence of air-sea transfer coefficients on bulk stability. *J. Geophys. Res.* **73**, 2549-2557.
- Denman, K. L. (1973). Time dependent model of the upper cone. *J. Phys. Oceanogr.* **3**, No. 2, 173-184.
- Dyer, K. R. (1974). The salt balance in stratified estuaries. *Estuarine Coastal Mar. Sci.* **2**, 273-281.
- Elder, R. A. and Wunderlich, W. O. (1972). Inflow density currents in TVA reservoirs. *Proc. Int. Symp. Stratified Flow*, Am. Soc. Civ. Eng.
- Ellison, T. H. and Turner, J. S. (1959). Turbulent entrainment in stratified flows. *J. Fluid Mech.* **6**, 423-448.
- Fischer, H. B., List, E. J., Koh, R. Y. C., Imberger, J. and Brooks, N. H. (1979). "Mixing in Inland and Coastal Waters." Academic Press, New York.
- Garrett, C. (1979). Mixing in the ocean interior. *Dyn. Atmos. Oceans* **3**, 239-256.
- Garrett, C. J. R. and Munk, W. H. (1975). Space-time scales of internal waves: a progress report. *J. Geophys. Res.* **80**, 291-297.
- Hebbert, B., Imberger, J., Loh, I. and Patterson, J. (1979). Collie River underflow into the Wellington Reservoir. *J. Hydraul. Div. Proc. Am. Soc. Civ. Eng.* **150**, HY5, 533-545.
- Hicks, P. B. (1972). Some evaluations of drag and bulk transfer coefficients over water bodies of different sizes. *Boundary-Layer Meteorol.* **3**, 201-213.
- Hicks, B. B. (1975). A procedure for the formulation of bulk transfer coefficients over water. *Boundary-Layer Meteorol.* **8**, 515-524.
- Huber, D. G. (1960). Irrotational motion of two fluid strata towards a line sink. *J. Eng. Mech. Div. Proc. Am. Soc. Civ. Eng.* **53**, No. 2, 329-349.
- Imberger, J. (1977). On the validity of water quality models for lakes and reservoirs. *Proc. Congr. Int. Assoc. Hydraul. Res. 17th* **6**, 293-303.
- Imberger, J., Patterson, J., Hebbert, B. and Loh, I. (1978). Dynamics of reservoir of medium size. *J. Hydraulic. Div. Proc. Am. Soc. Civ. Eng.* **104**, No. HY5, 725-743.
- Imberger, J. and Spigel, R. H. (1980). Billowing and its influence on mixed layer deepening. *Proc. Symp. Surf. Water Impoundments*, Minneapolis. In press.

- Imberger, J., Thompson, R. and Fandry, C. (1976). Selective withdrawal from a finite rectangular tank. *J. Fluid Mech.* **78**, 389-512.
- Koh, R. C. Y. (1966). Viscous stratified flow towards a sink. *J. Fluid Mech.* **24**, 555-575.
- Lawrence, G. A. and Imberger, J. (1979). Selective Withdrawal through a Point Sink in a Continuously Stratified Fluid with a Pycnocline. Department of Civil Engineering, University of Western Australia, Report No. ED-79-002.
- Lumley, J. L. (1965). On the interpretation of time spectra measured in high intensity shear flows. *Phys. of Fluids* **8**, 1056.
- Niiler, P. P. and Kraus, E. B. (1977). One-dimensional models of the upper ocean. In "Modelling and Prediction of the Upper Layers of the Ocean," (Ed. E. B. Kraus). Pergamon Press, New York.
- Ozmidov, R. V. (1965a). Some features of the energy spectrum of oceanic turbulence. *Dokl. Acad. Nauk. SSSR Earth Sci.* **160**, 11-18.
- Ozmidov, R. V. (1965B). On the turbulent exchange in a stably stratified ocean. *Atmos. Oceanic Phys.*, Ser. 1, 853-860.
- Pond, S., Fissel, D. B. and Paulson, C. A. (1974). A note on bulk aerodynamic coefficients for sensible heat and moisture fluxes. *Boundary-Layer Meteorol.* **6**, 333-339.
- Rayner, K. N. (1980). Diurnal Energetics of a Reservoir Surface Layer. Joint Report: Environmental Dynamics, Department of Civil Engineering, University of Western Australia, Report ED-80-005, and Department of Conservation and Environment, Western Australia, Bulletin No. 75.
- Sherman, F. S., Imberger, J., and Corcos, G. M. (1978). Turbulence and mixing in stably stratified waters. *An. Rev. Fluid Mech.* **10**, 267-288.
- Spigel, R. H. (1978). Wind Mixing in Lakes. Unpublished doctoral thesis, University of California, Berkeley.
- Spigel, R. H. and Imberger, J. (1980). The classification of mixed layer dynamics in lakes of small to medium size. *J. Phys. Oceanogr.* (in press).
- Swinbank, W. C. (1963). Longwave radiation from clear skies. *Quart. J. Roy. Meteorol. Soc.* **89**, 339-348.
- Thorpe, S. A. and Hall, A. J. (1977). Mixing in the upper layer of a lake during heating cycle. *Nature* **265**, 719-722.
- Tennessee Valley Authority (1972). Heat and Mass Transfer between a Water Surface and the Atmosphere. Division of Water Resources Research, Tennessee Valley Authority, Report No. 14.
- Wu, J. (1973). Wind induced entrainment across a stable density interface. *J. Fluid Mech.* **61**, 275-278.
- Zeman, O. and Tennekes, H. (1977). Parameterisation of the turbulent energy budget at the top of the daytime atmospheric boundary layer. *J. Atmos. Sci.* **34**, 111-123.